CHAPTER 6

Absorption of Nuclear Radiation

Contents

Our understanding of the nature of nuclear particles is based on their mode of interaction with matter. Knowledge about this interaction is essential in a variety of areas of nuclear science, such as the proper utilization and construction of detection and measuring devices for radiation, the design of radiation shielding, the medical and biological applications of radiation, radiochemical synthesis, etc.

The term *nuclear radiation* is used to include all elementary particles, both uncharged (e.g. photons) and charged, having energies in excess of approximately 100 eV whether the particles have been produced through nuclear reactions (spontaneous or induced) or have acquired their energy in electrostatic accelerators. This lower energy limit is very high in

TABLE 6.1. *Survey of nuclear radiation absorption processes*
The reaction cross sections (σ) give only order of magnitude at about 1 MeV in Z ≈ 20

	Reacting particles and fields	Type of reaction	σ (barns)	Name of process
1	*Protons and heavier ions* react with			
1a	orbital electrons	Particle energy loss through atomic excitation and ionization	$\geq 10^5$	Ionization, (atomic) excitation
1b	atomic nucleus	Particle elastically scattered	< 10	Nuclear scattering
1c	atomic nucleus	Particle inelastically scattered	< 1	Nuclear (coulomb) excitation
1d	atomic nucleus	Particle captured, formation of compound nucleus ($E_p > E_{cb}$(min)[c])	< 0.1	Nuclear transmutation
2	*Electrons* (e$^-$, β^-, β^+) react with			
2a	orbital electrons	Particle energy loss through atomic excitation and ionization	$\gg 10^2$	Ionization, (atomic) excitation
2b	orbital electrons	Slow β^+ annihilated, 2–3 photons formed	(100%)	Positron annihilation
2c	electric field of nucleus	Particle scattered with energy loss, continuous emission of $h\nu$($E_e \gg 1$ MeV)	$\gg 1$	Bremsstrahlung
3	*Photons* (γ) react with			
3a	field of orbital electrons	γ scattered without energy loss	≤ 0.01	Coherent scattering
3b	free (outer) electrons	γ scattered with energy loss, ionization	$< 10^{3}$[b]	Compton effect
3c	bound (inner) electrons	γ completely absorbed, one electron knocked out		Photo effect
3d	field of nuclear force	γ annihilated, formation of positron-negatron pair ($E_\gamma > 1.02$ MeV)		Pair formation
3e	atomic nucleus	γ scattered without energy loss	$\leq 10^{-3}$	Mössbauer effect
3f	atomic nucleus	γ scattered with energy loss		Nuclear excitation
3g	atomic nucleus	γ absorbed by nucleus, nuclear transmutation ($E_\gamma > 5$ MeV)[b]		Nuclear photo effect
4	*Neutrons* react with			
4a	atomic nucleus	n scattered with energy loss	≤ 10	Neutron moderation
4b	atomic nucleus	n captured, nuclear transformation	$< 10^4$	Neutron capture

[a] See Fig. 6.17; σ increases strongly with decreasing energy.
[b] Threshold energy for ^{9}Be(γ,α)^{4}He 1.6 MeV, ^{2}D(γ,n)^{1}H 2.2 MeV.
[c] E_{cb}(min) is the Coulomb barrier energy, eqn. (12.18).

comparison to ionization energies (usually < 15 eV) and to the energies involved in chemical bonds (normally 1 - 5 eV). Therefore, nuclear radiation can cause ionization in its passage through matter; this is reflected in the common name *ionizing radiation*. Neutrons of energies < 100 eV are included because their absorption (capture) by nuclei results in emission of nuclear radiation with energies $\gg 100$ eV.

The passage of such high energy radiation through matter results in the transfer of energy to the atoms and molecules of the absorber material. This transfer of energy continues until the impinging particle of the radiation has reached the same average kinetic energy as the atoms comprising the material; i.e. until *thermal equilibrium* is obtained.

In considering the absorption of nuclear radiation it is appropriate to view the overall process from two aspects: (1) processes occurring to the nuclear particles themselves as their energies are reduced to the thermal equilibrium value; such *absorption processes* are the principal consideration of this chapter; (2) processes in the absorbing material due to the effect of the transfer of energy. This transfer results initially in excitation and ionization which cause physical and chemical changes. The study of these effects is the domain of *radiation chemistry* and is considered in Chapter 7.

6.1. Survey of absorption processes

The reduction in the intensity of a beam of ionizing particles can be caused either by reaction with the nuclei of the absorbing material (nuclear reactions) or with the atomic electrons (electron collision). In Table 6.1 the most important processes involved in the absorption of nuclear radiation in matter are listed along with the probability for each process. Comparison shows that the probability of interactions with electrons is considerably greater than that of a nuclear reaction; the only exception to this is the case of neutron absorption. In fact the principal mode of interaction between the particle and the atoms of the absorbing material involves the electromagnetic fields of the particle and the atomic electrons. Since neutrons are neutral particles, in order for them to transfer energy it is necessary that they experience a collision with a nucleus. Consequently for all particles except neutrons, nuclear reactions can be neglected in considering the processes involved in the reduction of the intensity of the particle beam.

As nuclear radiation passes the atoms of an absorber, it can transfer some of its energy to the atoms. If the amount of energy transferred is sufficient, ionization of the atom results. The positive ion and the electron thus formed are known as an *ion pair*. Frequently the electrons from this primary ionization have sufficiently high kinetic energy to cause *secondary ionization* in other atoms. The number of electrons produced in secondary ionization is often larger than that of the primary ionization but the average kinetic energies of the secondary electrons are lower than those of the primary electrons. In many interactions the initial radiation transfers insufficient energy for ionizations; instead an electron is raised to a higher, excited energy level of the atom. These *excited atoms* rapidly return to lower energy states by emission of electromagnetic radiation such as X-rays, visible light, etc. For neutrons the absorption process involving the capture of the neutron (cf. §§4.5 and 10.6) imparts sufficient recoil energy to cause ionization and excitation.

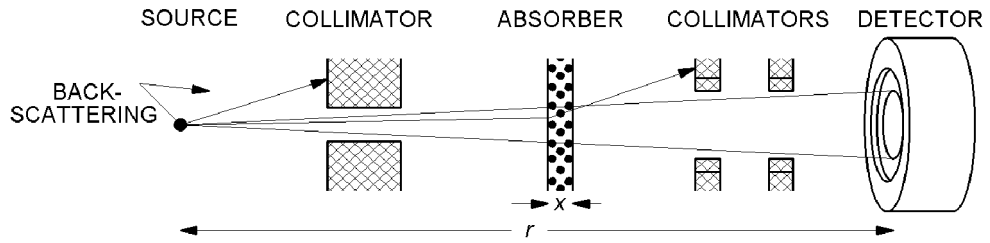

FIG. 6.1. Geometrical arrangement for measuring absorption curves.

6.2. Absorption curves

In order to measure the absorption of nuclear radiation, the experiments must be performed in such a manner as to eliminate as many of the interfering factors as possible. Usually a well-collimated beam is used. This is illustrated in Figure 6.1 for a point radioactive source. The relation between the disintegration rate A and the count rate R is given by (4.45):

$$R = \psi A$$

The *counting efficiency* ψ includes a number of factors:

$$\psi = \psi_{sample}\, \psi_{abs}\, \psi_{det}\, \psi_{geom} \tag{6.1}$$

If conditions were ideal, there would be no self-absorption or scattering in the sample (in which case $\psi_{sample} = 1$), no absorption of radiation between the sample and the detector window ($\psi_{abs} = 1$), and the detector would have a 100% efficiency (sensitivity) to a "count" for each particle reaching its window ($\psi_{det} = 1$).

The geometric efficiency ψ_{geom}, is 1 for 4π-geometry, i.e. for a spherical detector subtending a 360^{o} solid angle about the sample. Although such detectors exist (Ch. 8), more commonly the sample is counted outside the detector at some distance r, as indicated in Figure 6.1. If the detector window offers an area of S_{det} perpendicular to the radiation, the geometrical efficiency is approximated by (for small ψ_{geom})

$$\psi_{geom} \approx S_{det}/(4\pi r^{2}) \tag{6.2}$$

If a detector with a circular window of radius s is at a distance r from a source of radius d, the geometrical efficiency is given by

$$\psi_{geom} = \tfrac{1}{2}[1 - (1 + s^{2}/r^{2})^{-\frac{1}{2}}]\, k \tag{6.3}$$

When the sample is a point source, $k = 1$, else k can be read from the series of curves in Figure 6.2.

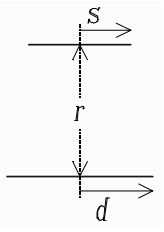

The activity measured is proportional to the particle flux ϕ reaching the detector

$$R = k_{det}\,\phi \tag{6.4}$$

where $k_{det} = S_{det}\,\psi_{det}$ and

$$\phi = \psi_{abs}\,\phi_0 \tag{6.5}$$

and

$$\phi_0 = \psi_{sample}\,nA/(4\pi r^2) \tag{6.6}$$

ϕ_0 is the flux of particles (particles $m^{-2}\,s^{-1}$) which reach the detector from the source when $\psi_{abs} = 1$, and n is the number of particles emitted per decay ($n > 1$ only for γ following α- and β-decays). Thus if every β-decay yields 2γ (in cascade) and γ is the measured radiation, then $n_\gamma = 2$, and $\phi_0 = n_\gamma A_\beta/(4\pi r^2)$ γ-quanta $m^{-2}\,s^{-1}$. In branched decay n will not be an integer. Equation (6.6) is the so called $1/r^2$ *-law* since the measured flux varies as the inverse of the square of the distance to the source.

These equations are valid as long as the conditions at the source and at the detector, as well as r, are kept constant. When an absorber is inserted between the source and detector (Fig. 6.1), ψ_{abs} depends on the absorber thickness x (m). For zero absorber thickness, $\psi_{abs} = 1$ in accurate measurements. There is a small absorption due to the air between the sample and detector unless the measurement is done in a vacuum.

Absorption curves relate the variation of either R or ϕ to the thickness of the absorbing material. In Figure 6.3 the relative transmission ϕ/ϕ_0 is plotted as a function of absorber thickness for different kinds of radiation. For charged particles, i.e. electrons, protons, and heavier ions, ϕ/ϕ_0 reaches zero at a certain x-value (x_{max}); this is referred to as the maximum range, R, of the particles. The range can be expressed by either the *average range* ($x = C_1$ for heavy ions and C_3 for electrons) or the *maximum* (or extrapolated) *range* (C_2 and C_4, respectively, in Fig. 6.3). The loss of energy involves collisions with atomic electrons, and the energy loss per collision and the number or collisions varies from one ionizing particle to the next, resulting in a slight *straggling* in the range. The average range is the meaningful one.

Figure 6.4 shows an absorption curve for ^{32}P. The radioactivity R has been measured as a function of aluminum absorber thickness in *linear density*, kg m^{-2} or more commonly mg cm^{-2}. The low activity "tail" (C_4 in Fig. 6.4) is the background activity R_b, which has to be subtracted from the measured value R_m to obtain the true value for the radiation (e.g. ^{32}P): $R = R_m - R_b$. The extrapolation of R to a value equal to R_b (i.e. C_3) gives the range.

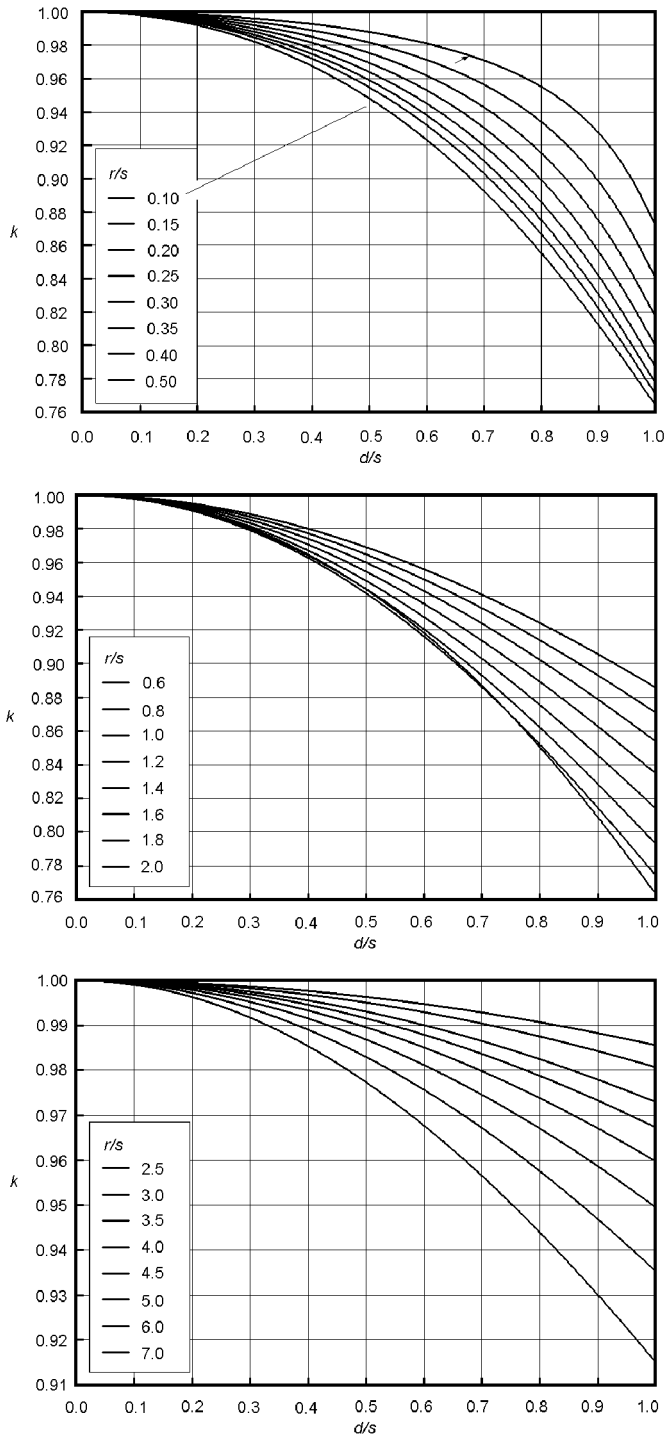

FIG. 6.2. Correction factor for finite source radius, eqn. (6.3).

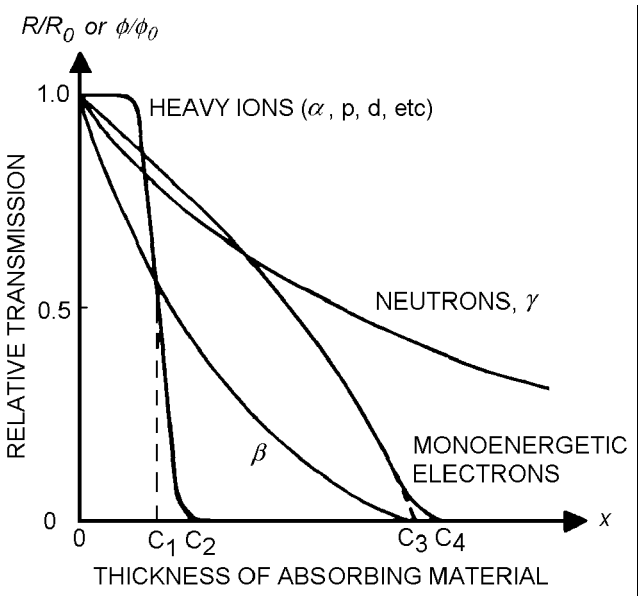

FIG. 6.3. Curves showing relative transmission ϕ/ϕ_0 (or R/R_0) as function of absorber thickness x. C_1 and C_3 are average, C_2 and C_4 maximum range.

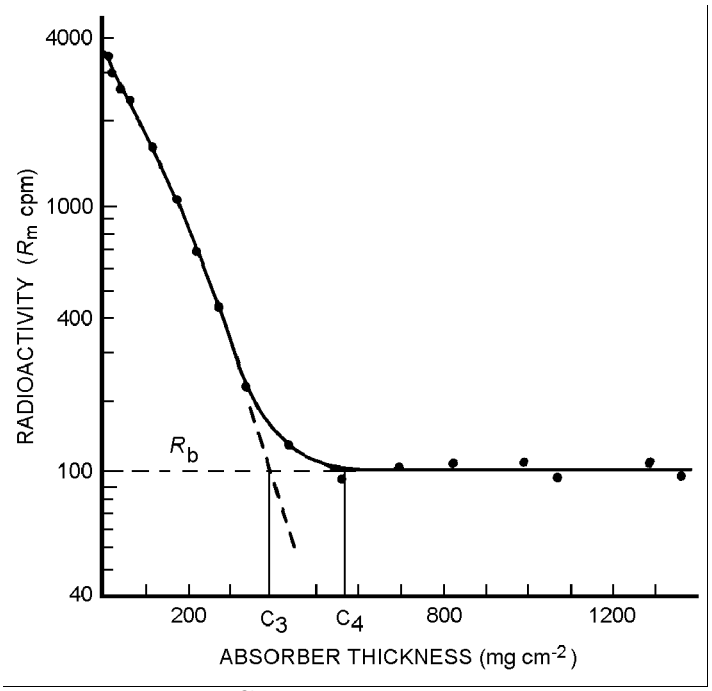

FIG. 6.4. Absorption curve for ^{32}P β-radiation showing extrapolated (C_4) and average (C_3) ranges. The dashed curve is obtained after subtraction of background.

Whereas it is possible to specify maximum ranges for charged particles, this is not possible for neutral particles such as neutrons and γ-quanta. If the absorber is not too thick, these particles undergo only one collision, or at the most a few, before they are absorbed. As a result the absorption curve has an exponential form.

$$\phi = \phi_0 e^{-\mu x} \tag{6.7}$$

where μ is the *total attenuation coefficient*. Thus for n and γ we have

$$\psi_{abs}(x) = e^{-\mu x} \tag{6.8}$$

The reduction in intensity of a beam can occur by two mechanisms. One involves the deflection or scattering of the particles from the direct line of path between the source and the detector and is described by the *scattering coefficient* μ_s. The second mode of reduction is the complete transfer of the projectile energy to the absorbing material (the particles are "captured") and is designated by the (*energy*) *absorption coefficient* μ_a. The (total) attenuation coefficient in (6.7) is the sum of both these modes.

$$\mu = \mu_s + \mu_a \tag{6.9}$$

Both μ_s and μ_a can be measured independently. The (total) attenuation coefficient is of primary interest in radiation shielding, while the (energy) absorption coefficient is important in considering radiation effects on matter.

6.3. Absorption of protons and heavier ions

The mode of interaction of protons and heavier charged particles with the atoms of the absorbing material can be illustrated by considering the absorption of α-particles. With rare exception, α-particles emitted by radioactive nuclides have energies between 4 and 9 MeV. Since the α-particles are so much heavier than electrons, they are deflected very slightly when their Coulomb fields interact with atoms or molecules to form ion pairs. As a result, α-particles travel in a straight line as they pass through matter, which explains the straight paths observed for α-particles in cloud chamber photographs (Fig. 6.5). This is in contrast to the very curved or irregular paths of the secondary electrons emitted in the formation of the ion pair. For a 5 MeV α-particle the maximum energy of the secondary electrons is 2.7 keV. However only a small fraction of the secondary electrons actually receive this much energy; the average energy of the secondary electrons is closer to 100 eV. The ionization caused by more energetic secondary electrons is usually referred to as δ-*tracks* (cf. §7.2).
In solids and liquids the total path length for α-particles from radioactive decay is quite short. However, in gases at standard temperature and pressure the paths are several centimeters long (Table 6.2). The range in air for α-particles with an initial energy E_α MeV can be calculated by the empirical equation ($\rho_{air} = 1.293$ kg m^{-3}):

$$R_{air} = 0.31 E_\alpha^{3/2} \text{ (cm)} = 0.40 E_\alpha^{3/2} \text{ (mg cm}^{-2}\text{)} \tag{6.10}$$

The range R_z in other materials can be approximated roughly by

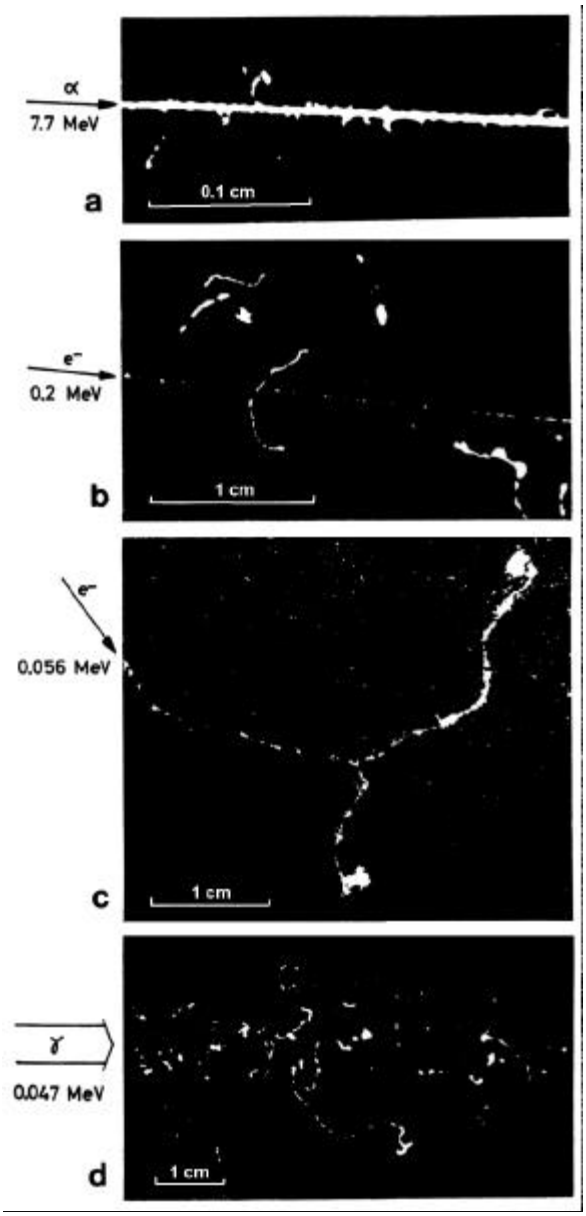

FIG. 6.5. Cloud chamber tracks of α, β, (e^-) and γ-rays at 1 bar in air ((a), (b), and (c)) and in methane (d). (From W. Gentner, H. Maier-Leibnitz, and H. Bothe.)

$$R_z = 0.173\, E_\alpha^{3/2} A_z^{1/3} \text{ (mg cm}^{-2}\text{)} \tag{6.11}$$

TABLE 6.2. *Range in water, and average linear energy transfer (LET) values for different radiation*

Upper half refers to monoenergetic (accelerated) particles. For β-decay $E_{abs} = 1/3\ E_{max}$

Radiation	Energy (MeV)	Maximum range		Average LET value in water (keV/μm)
		cm air	mm water	
Electron	1	405	4.1	0.24
	3	1400	15	0.20
	10	4200	52	0.19
Proton	1	2.3	0.023	43
	3	14	0.014	21
	10	115	1.2	8.3
Deuteron	1	1.7	–	–
	3	8.8	0.088	34
	10	68	0.72	14
Helium	1	0.57	0.0053	190
	3	1.7	0.017	180
	10	10.5	0.11	92
Fiss. fragment	100	2.5	0.025	3300
^{226}Ra (α)	E_α 4.80	3.3	0.033	145
^{210}Po (α)	E_α 5.30	3.8	0.039	136
^{222}Rn (α)	E_α 5.49	4.0	0.041	134
^{3}H (β)	E_{max} 0.018	0.65	0.0055	1.1
^{35}S (β)	E_{max} 0.167	31	0.32	0.17
^{90}Sr (β)	E_{max} 0.544	185	1.8	0.10
^{32}P (β)	E_{max} 1.71	770	7.9	0.07
^{90}Y (β)	E_{max} 2.25	1020	11	0.07
^{137}Cs (γ)	E_γ 0.66	$x_{½}$ = 8.1 cm H_2O	0.39	
^{60}Co (γ)	E_γ 1.20-1.30	$x_{½}$ = 11.1 cm H_2O	0.27	

where A_z is the atomic weight of the absorber. Figure 6.6 shows the range of various charged particles in an aluminum absorber. The range of a 5 MeV α is 6 mg cm^{-2}; thus $R_{Al} = 6 \times 10^{-3}/\rho_{Al}$ cm = 0.002 mm. Alpha-particles from radioactive decay are easily stopped even by the thickness of a sheet of paper.

When the absorber consists of a composite material, containing the weight fractions w_1, w_2, w_3, etc of elements 1, 2, 3, etc with ranges R_1, R_2, R_3, etc, the range R_{comp} in the absorber is obtained from the relation

$$1/R_{comp} = w_1/R_1 + w_2/R_2 + w_3/R_3 + \cdots \tag{6.12}$$

The number of ion pairs formed per millimeter of range for α-particles, protons, and electrons are shown in Figure 6.7a. The larger *specific ionization* of the α-particles compared to the protons is related to the fact that the former are doubly charged. In general the specific ionization increases with the ionic charge of the particle for the same kinetic energy. Fission fragments that initially have very large energies also have very large ionic charges leading to quite high specific ionization in their absorption in matter; their range is 2-3 cm in air and 2-3 mg cm^{-2} in aluminum.

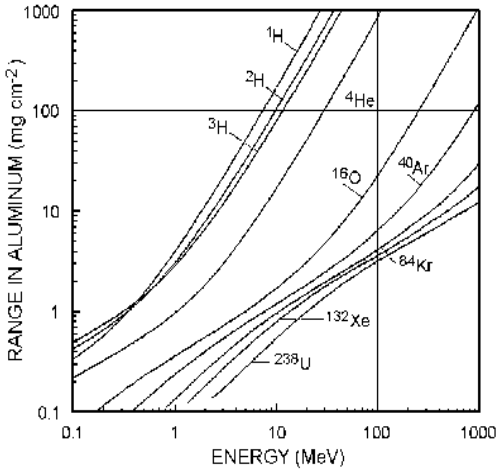

FIG. 6.6. Range of some energetic particles in an aluminum absorber.

A quantum-mechanical and relativistic analysis of the interaction between a fast moving positive ion of atomic number z and the electrons in the absorber leads to the following expression for the energy loss per unit distance, dE/dx (J/m), traveled in an absorber

$$-dE/dx = \{(4\pi\gamma^2 z^2 \mathbf{e}^4 NZ)/(\mathbf{m}_e v^2)\}[\ln\{(2\mathbf{m}_e v^2)/I\} - \ln(1-\beta^2) - \beta^2] \tag{6.13}$$

where $\gamma z\mathbf{e}$ is the charge of the ion moving at velocity v ($\beta = v/\mathbf{c}$) through an absorber containing N atoms of atomic number Z per volume unit and having an effective ionization potential I. For a completely stripped ion, $\gamma = 1$. The range, R, of an ion may be calculated by integrating the energy loss expression

$$R = \int_{E_0}^{0} (dE/dx)^{-1}\, dE \tag{6.14}$$

from the initial energy E_0 to zero.

Charged particles decrease in velocity as they lose their energy in traversing an absorber. As a result they spend progressively longer times in the vicinity of any particular atom, which results in an increase in the probability of interaction with that atom. Consequently there is a steady increase in the number of ion pairs formed along the path of the particle rather than a constant density of ion pairs. Near the end of the range for heavy charged particles a maximum is observed for the number of ion pairs formed per unit path length (the *Bragg peak*) (Fig. 6.7b). At a distance just beyond the Bragg peak maximum the kinetic energy of the particles is comparable to those of the orbital electrons of the absorber. As a result, the particle can acquire electrons, $\gamma < 1$ in (6.13), finally becoming uncharged, $\gamma = 0$, and thereby losing its ability to cause further ionization.

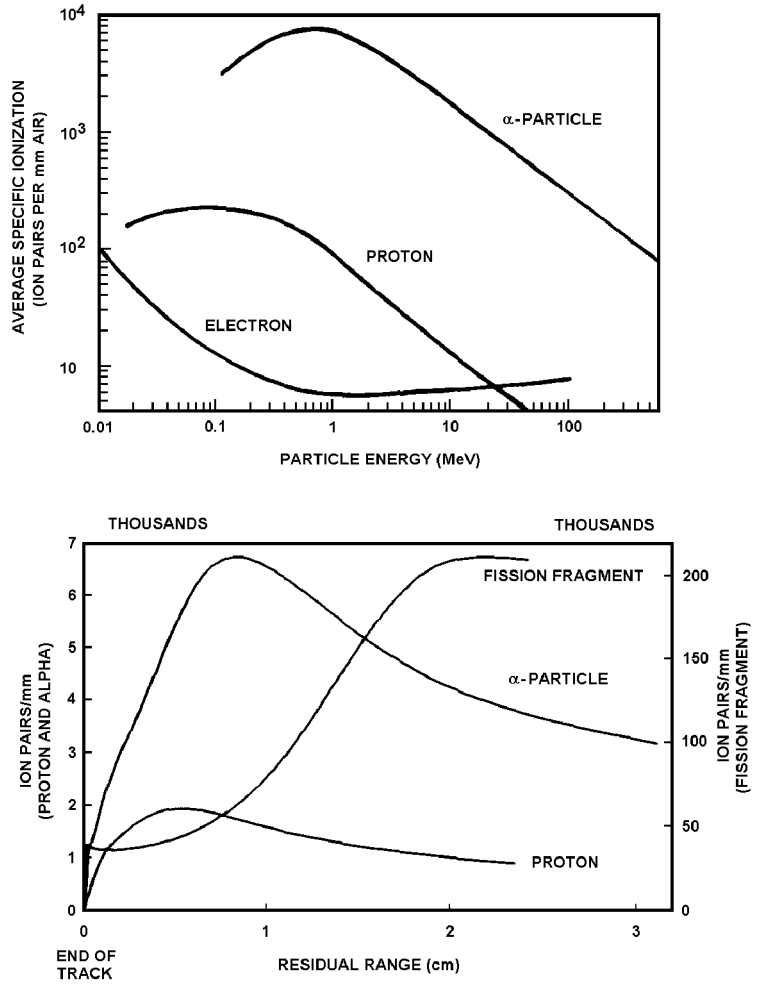

FIG. 6.7. Number of ion pairs formed per mm air at STP as function of particle energy. (a) average specific ionization at maximum particle energy, (b) same for residual range. (From H. A. C. McKay.)

6.4. Absorption of electrons

Absorption of high energy electron beams occurs through interaction with the orbital electrons and the electromagnetic field at the atom. The processes are summarized in Table 6.1 and Figure 6.8. In order to distinguish between electrons from accelerators and those from β-decay we refer to the latter as β-*particles*.

6.4.1. *Ionization*

Beta-particles lose their energy primarily by the same mechanism as α-particles (Fig. 6.7a and b); however, there are several important differences. Since the masses of the β-particles and of the orbital electrons are the same at non-relativistic velocities, the β-particles can lose a large fraction of their energy in a single collision. The β-particle undergoes a wide angle deflection in such collisions and consequently β-particles are scattered out of the beam path all along the length. The secondary electrons ionized from the atom have such high energies that they cause extensive secondary ionization which provides 70-80% of the total ionization in β-absorption processes (Fig. 6.5b). Approximately half of the total

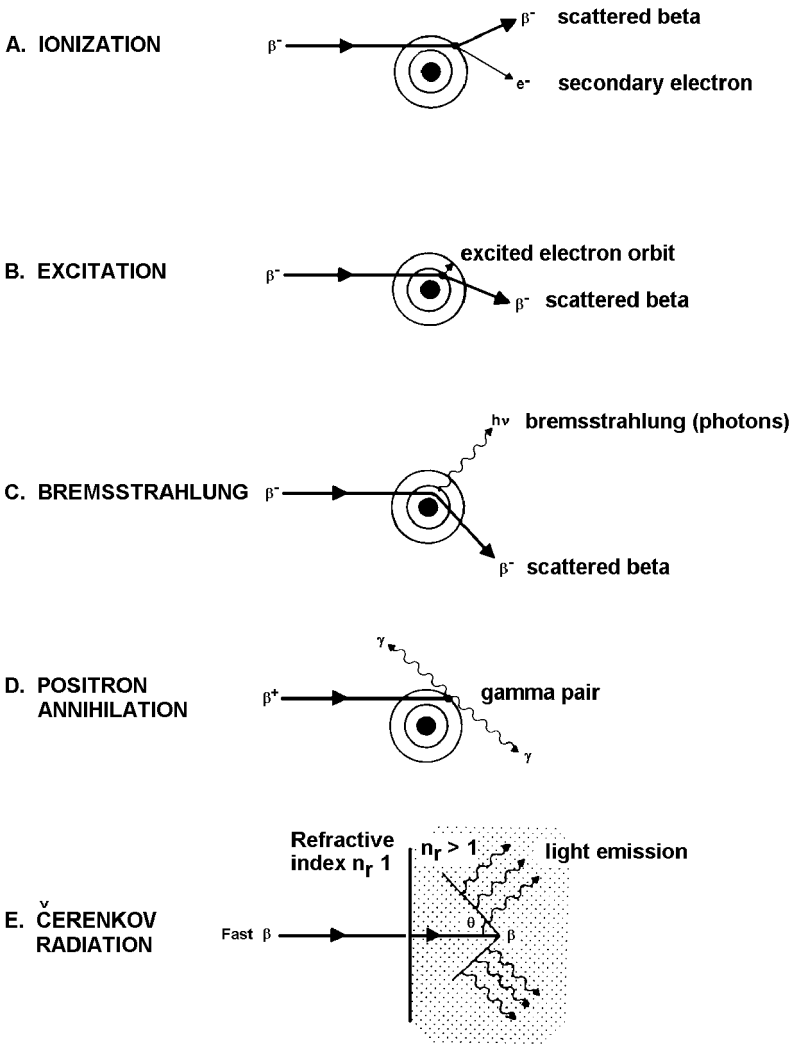

FIG. 6.8. Schematic description of the five processes accounting for β-particle absorption.

energy of the β-particle is lost by ionization and half by excitation. The track formed is further discussed in §7.2.

The specific ionization from a β-particle is much lower than that from a heavy ion as can be seen in Figure 6.7a. This is due to the fact that for the same initial energy, β-particles have much greater velocity than have α-particles or protons because their mass is very much smaller than the mass of the heavy particles. This greater velocity results in a correspondingly lower ionization and gives a much longer range to β-particles. The erratic path observed for β-particles in Figure 6.5c is a result of the large energy transfer and the resulting large deflections involved in the encounters with the orbital electrons. However, at very high energies the β-particles have straight paths as a result of the fact that very energetic β-particles have a momentum considerably in excess of that of the orbital electron.

6.4.2. *Bremsstrahlung*

As a β-particle approaches an atomic nucleus, it is attracted by the positive field of the nucleus and deflected from its path. The deflection results in an acceleration that, according to classical electrodynamics, leads to emission of electromagnetic radiation (Fig. 6.8c). Therefore the encounter with the positive charge of the nuclear field decreases the energy of the β-particle by an amount exactly equal to the amount of electromagnetic radiation emitted. This radiation is known as *bremsstrahlung* (braking radiation). The loss of energy by emission of bremsstrahlung radiation increases with the β energy and with the atomic number of the absorber material (Fig. 6.9). In aluminum approximately 1% of the energy of a 1 MeV electron is lost by bremsstrahlung radiation and 99% by ionization whereas in lead the loss by radiation is about 10%. For electrons of greater than 10 MeV energy,

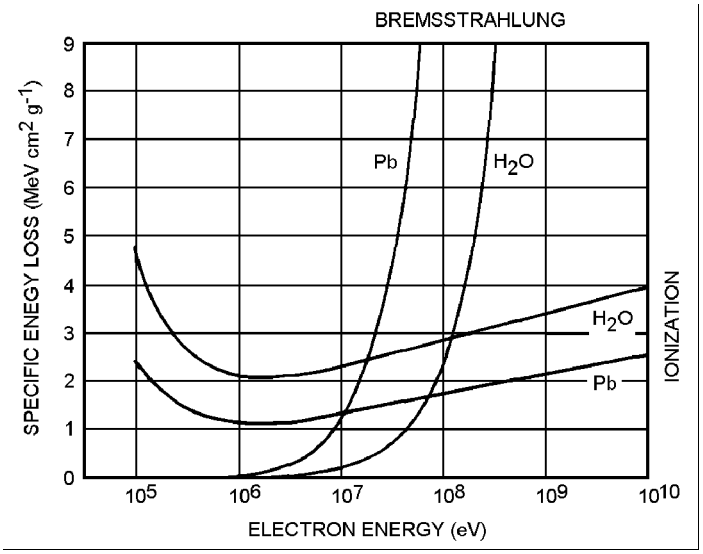

FIG. 6.9. Energy loss of fast electrons by ionization and bremsstrahlung. (From Gentner, Maier-Leibnitz, and Bothe.)

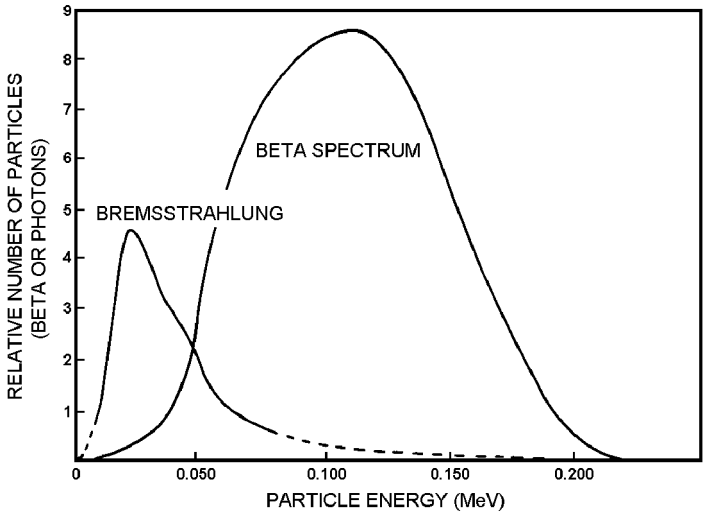

FIG. 6.10. Beta-spectrum (right curve) and bremsstrahlung spectrum in aluminum for ^{147}Pm. The ordinate of the bremsstrahlung spectrum is enlarged about 100 times.

bremsstrahlung emission is the predominant mode of energy loss in lead. However, for the energies in radioactive decay, bremsstrahlung can usually be neglected - particularly for absorption processes in material of low atomic weight. The ratio of *specific energy loss* (dE/dx) through bremsstrahlung to that through collision (i.e. all other processes) is approximately:

$$(\mathrm{d}E/\mathrm{d}x)_{\mathrm{brems}} / (\mathrm{d}E/\mathrm{d}x)_{\mathrm{coll}} \approx E_{\mathrm{e}}\, Z/800 \tag{6.15}$$

where E_{e} is kinetic energy of the electron (MeV) and Z the atomic number of the absorber atoms.

Figure 6.10 shows the bremsstrahlung spectrum obtained in aluminum for β-particles emitted by ^{147}Pm. In this case a very small fraction of the β-energy is converted into radiation. The bremsstrahlung spectrum is always of much lower energy than that of the β-spectrum. Bremsstrahlung sources of a wide variety of energies are commercially available. Recently special electron accelerators have been designed for the sole purpose of producing bremsstrahlung radiation to be used for (analytical) X-ray excitation and for medical irradiation purposes; see Ch. 13.

6.4.3. *Cerenkov radiation*

The velocity of light in matter c depends on the refractive index n_{r}

$$c = \mathbf{c}\, n_{\mathrm{r}}^{-1} \tag{6.16}$$

In water $n_{\mathrm{r}} = 1.33$, in plexiglass 1.5. β-particles with energies > 0.6 MeV move faster than light in water. When the particle velocity (v_{p}) > c, electromagnetic radiation is

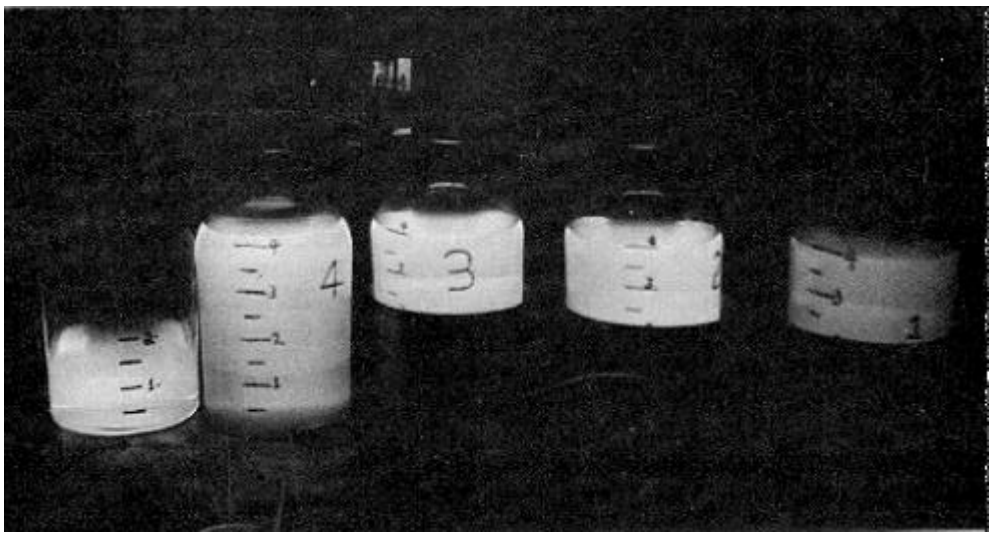

FIG. 6.11. Bottles containing highly radioactive ^{90}Sr solutions glow in the dark due to Cerenkov radiation from daughter ^{90}Y (E_{max} 2.3 MeV).

emitted coherently in a cone whose axis is the direction of the moving particle (Fig. 6.8e). The angle of the cone θ is obtained from

$$\sin \theta = c/v_p \tag{6.17}$$

This Cerenkov radiation is the source of the bluish light observed in highly radioactive solutions (Fig. 6.11) and around reactor fuel elements submerged in water. The radiation can be used for detecting β-particles and for measuring high particle energies (from θ). For a fast electron the energy loss through Cerenkov radiation is ≤ 0.1% of the energy loss through other processes. Cerenkov detectors are described in Ch. 8.

6.4.4. *Positron annihilation*

Positrons interact with matter through ionization, excitation, emission of bremsstrahlung, and Cerenkov radiation in the same manner as negative electrons. As the kinetic energy of the positron decreases in the absorber, there is an increase in probability of direct interaction between the positron and an electron (Fig. 6.8d) in which both the positron and electron are annihilated. The energy of the two electron masses is converted into electromagnetic radiation. This process, known as *positron annihilation*, is a characteristic means of identification of positron emission. Since an electron mass is equivalent to 0.51 MeV, and the kinetic energy of the particles of annihilation is essentially zero, the total energy for the annihilation process is 1.02 MeV. In order to conserve momentum the photons must be emitted with equal energy and in exactly opposite direction in case of only two photons (the dominating case). These photons of 0.51 MeV each are referred to as *annihilation radiation*. The presence of γ-rays at 0.51 MeV in the electromagnetic spectrum

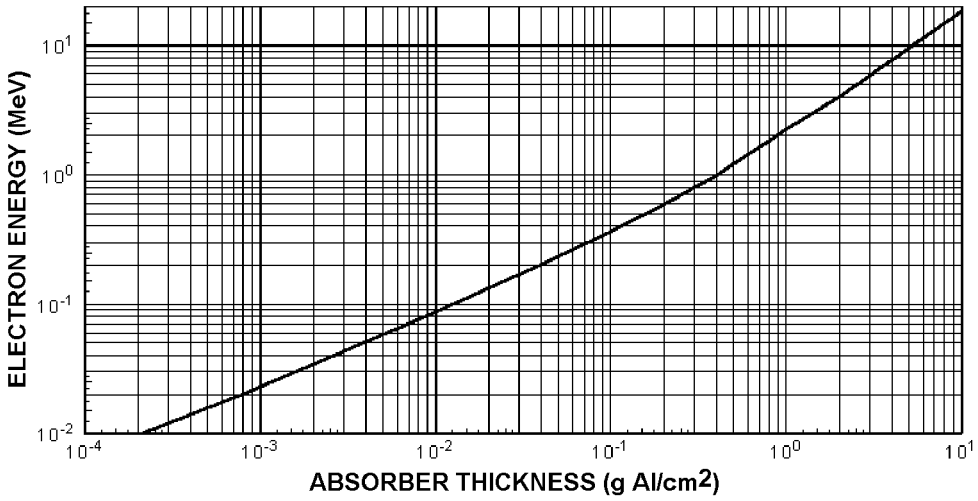

FIG. 6.12. Empirical relation for the maximum range of β-particles in aluminum.

of a radionuclide is strong evidence for the presence of positron emission by that nuclide.

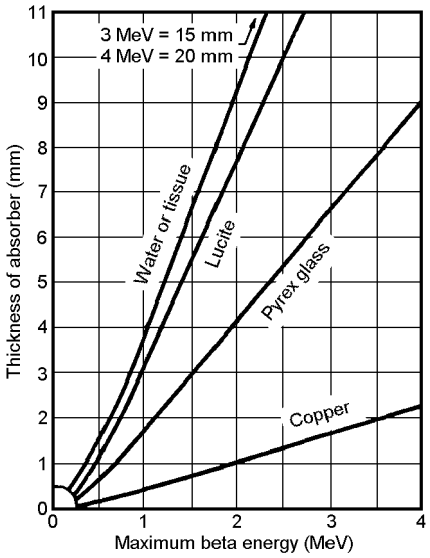

FIG. 6.13. Thickness of various materials needed to completely stop β-particles.

6.4.5. *Absorption curves and scattering of* β*-particles*

An absorption curve for β-particles has a quite different shape than it has for α-particles (cf. Fig. 6.3). The continuous spectrum of energies in radioactive β-decay plus the extensive wide angle scattering of the β-particles by the absorber atoms account for the fact that range curves for β-particles continuously decrease. Even for a beam of initially mono-energetic electrons, the continuous removal of electrons from the beam path by wide angle deflection results in a plot showing a continuous decrease in the numbers of electrons with distance, with approximately 95% of the original β-particles stopped in the first half of the range. It is more common to speak of the absorber thickness necessary to stop 50% of the particles than to speak of the range itself. This *half-thickness value* is much easier to ascertain experimentally than is an apparent range. It should be remembered that the energy deposited at complete β-absorption is $E_{abs} \approx E_{max}/3$ (Ch. 4).

The absorption curve for β-particles formed in radioactive decay can be described with fair approximation by the relationship (6.7). This is due to the continuous energy spectrum resulting in an exponential relationship for the range curve. In the E_{max} range 0.7-3 MeV the range in aluminum closely follows the relation (*Feather's rule*)

$$R(\text{g Al cm}^{-2}) = 0.543\,E_{max}(\text{MeV}) - 0.160 \qquad (6.18)$$

This is the range C_3 in Figure 6.4.

Figure 6.12 shows an empirical relationship between the maximum energy of β-particles and the extrapolated range in aluminum. Compared to α-radiation, β-radiation has a much longer range. For example, the range of an α-particle of 5 MeV is 3.6 cm in air while that of a β-particle of 5 MeV is over 17 m. A comparison of the range in air and water for electrons and heavy particles is given in Table 6.2. Figure 6.13 is useful for a rapid estimate of the absorber thickness needed to protect against β-particles.

An additional complication in the experimental measurements of absorption curves for β-particles is found in the fact that a certain fraction of β-particles which are not originally emitted in the direction of the detector may be deflected to the detector by the large angle

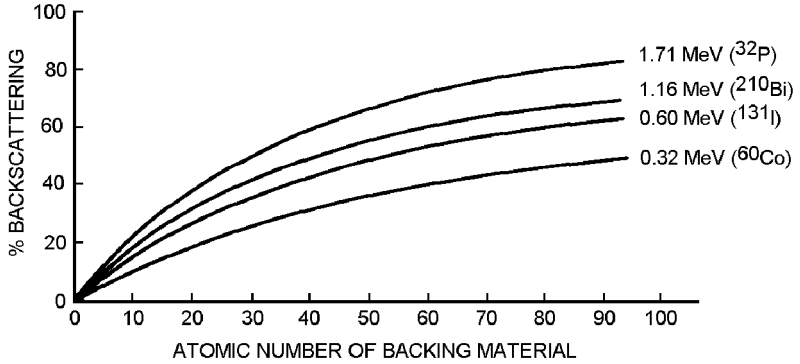

FIG. 6.14. Backscattering of β-particles of different energy as function of the atomic number of thick backing materials.

scattering. This process is known as *backscattering*, since the *backing* (or *support*) for radioactive samples may cause scattering of a certain fraction of the particles through as much as 180°. The fraction of back-scattered β-radiation depends on the geometry of the measuring system, the energy of the β-particles, and the thickness and electron density of the backing material. In Figure 6.14 the percent backscattering as a function of the atomic number of the backing material is shown for four β-energies (E_{max}); the radioactive sample is considered infinitely thin (i.e. no self-absorption). From the curve for ^{32}P on platinum ($Z = 78$) we see that about 40% of the measured radiation is due to back-scattered radiation (0.8/(1.0 + 0.8) = 0.4). Backscattering increases with the thickness of the backing material up to a saturation value which is reached when the thickness of the backing is about one- fifth of the extrapolated range of the β-particles in that material.

6.5. Absorption of γ-radiation

The absence of charge and rest mass for γ-rays results in little interaction with the absorbing atoms and in long ranges. The number of ion pairs produced in a given path length by γ-rays is only 1-10% of that produced by β-particles of the same energy (Fig. 6.5); e.g. a 1 MeV γ-ray produces only about one ion pair per centimeter of air. As a consequence of this low specific ionization of γ-rays, the ionization is almost completely secondary in nature resulting from the action of a few high energy primary ion pairs.

6.5.1. *Attenuation coefficient*

Unlike heavy particles and electrons which lose their energy as a result of many collisions, γ-rays are completely stopped in one or, at most, a few interactions. For thin absorbers the attenuation of γ-rays follows relation (6.7), where ϕ is the number of photons $m^{-2}\,s^{-1}$. The proportionality factor μ is called the (*total*) *attenuation coefficient*. When it has the dimension of m^{-1} and the thickness x is expressed in meters, μ is referred to as the *linear* attenuation coefficient. The attenuation coefficient can be expressed in other ways:

$$\mu_m = \mu/\rho = {}_a\mathbf{N}_A/M = {}_e Z\mathbf{N}_A/M \qquad (6.19)$$

where ρ is the density, M the average atomic weight, and Z the average atomic number of the absorber. $\mathbf{N}_A\rho/M$ can be replaced by N_v, by which we can define a *macroscopic absorption cross-section* (cf. §14.1). $^{-1}$ is the mean free path or *relaxation length* of the radiation in the absorbing material. μ_m (in $cm^2\,g^{-1}$ when x is in centimeters) is the *mass attenuation coefficient*; $_a$ is the probability of reaction between a γ-ray and the electron cloud of the absorber atom (*atomic reaction cross-section*, m^2 $atom^{-1}$); $_e$ is the probability of the reaction of a γ-ray with a single electron of the absorber (*electron reaction cross-section*, m^2 $electron^{-1}$). $_a$ and $_e$ are analogous to the nuclear reaction cross-sections discussed later. In Table 6.1 only the equivalent nuclear and atomic reaction cross-sections are given.

Since a γ-ray may be removed from the beam in the first few Ångströms of its entrance into the absorber or may travel several centimeters with no interaction at all and then be

removed, it is not possible to apply the range concept to γ-rays in the way that it is applied to charged particles. However, it is experimentally easy to measure the thickness of absorber necessary to remove half of the initial γ-rays (half thickness value) from a beam, or reduce it to 1/10, 1/100, etc. Figure 6.15 shows the required thickness of concrete and lead necessary to reduce γ-rays of different energies by factors of 10 (shielding thicknesses are further discussed in §6.7). The half-thickness value is

$$x_{½} = \ln(2)/\mu \tag{6.20}$$

and the 1/10 value

$$x_{1/10} = \ln(10)/\mu \tag{6.21}$$

6.5.2. *Partial absorption processes*

Gamma-ray absorption occurs as illustrated in Figure 6.16 by four different processes: coherent scattering, photoelectric effect, Compton effect, and pair production. For each of these processes, a partial coefficient can be expressed:

$$\mu = \mu_{coh} + \mu_{phot} + \mu_{Comp} + \mu_{pair} \tag{6.22}$$

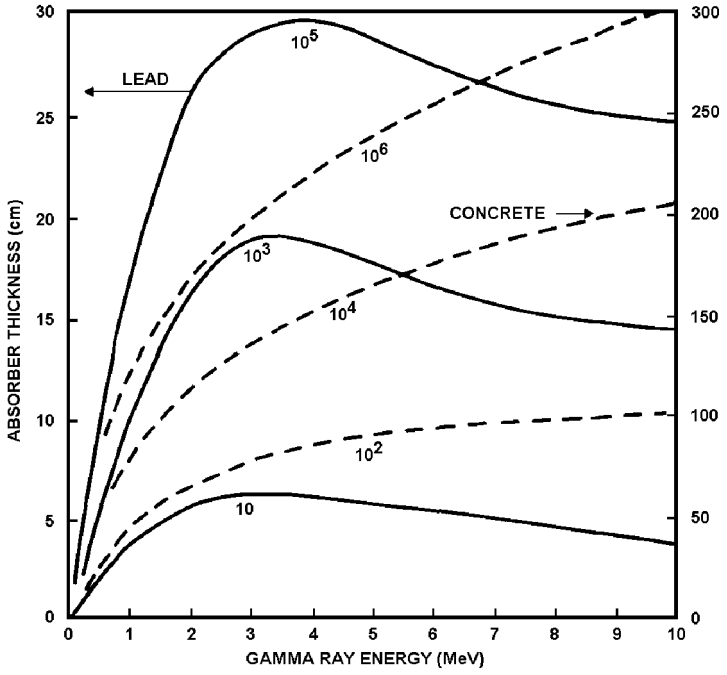

FIG. 6.15. Thickness of lead and concrete reducing γ-ray flux by different powers of 10, as function of γ-ray energy. The curves are for thick absorbers and include build-up factors.

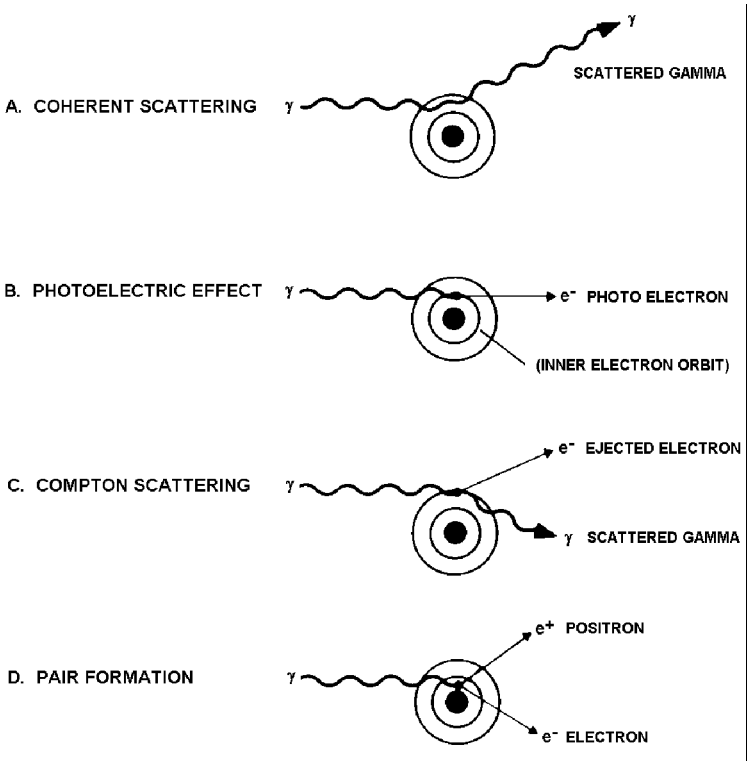

FIG. 6.16. Schematic description of the four main processes accounting for γ-ray interaction and absorption.

Comparing with (6.9), μ_{phot} and μ_{pair} are absorption processes, while μ_{coh} is all scattering; μ_{Comp} contributes to both the μ_s and the μ_a terms. In Figure 6.17 the total attenuation, absorption, and the partial coefficients are given for water, aluminum, and lead as a function of the γ-ray energy. The corresponding linear coefficients are obtained by multiplying with ρ (for aluminum 2.7, for lead 11.3). It should be noted that the aluminum curves also can be used for absorption in concrete.

In *coherent scattering* (also called Bragg or Rayleigh scattering, denoted $_r$ in Fig. 6.17) the γ-ray is absorbed and immediately re-emitted from the atom with unchanged energy but in a different direction. Coherently scattered radiation can give interference patterns, so the process is used for structural analysis of absorbing material in the same way as X-rays are. The probability for coherent scattering increases with the square of atomic number of the absorber and decreases with γ-ray energy. In lead, coherent scattering amounts to about 20% of the total attenuation for γ-energies of 0.1 MeV but decreases in importance for higher energy γ-rays.

In absorption of γ-rays by the *photoelectric effect* (denoted in Fig. 6.17) the photons are absorbed completely by the atom. This absorption results in excitation of the atom above the binding energy of some of its orbital electrons with the result that an electron is ejected and an ion pair formed. The energy E_e of the emitted photoelectron is the difference between the energy of the γ-ray and the binding energy for that electron in the atom.

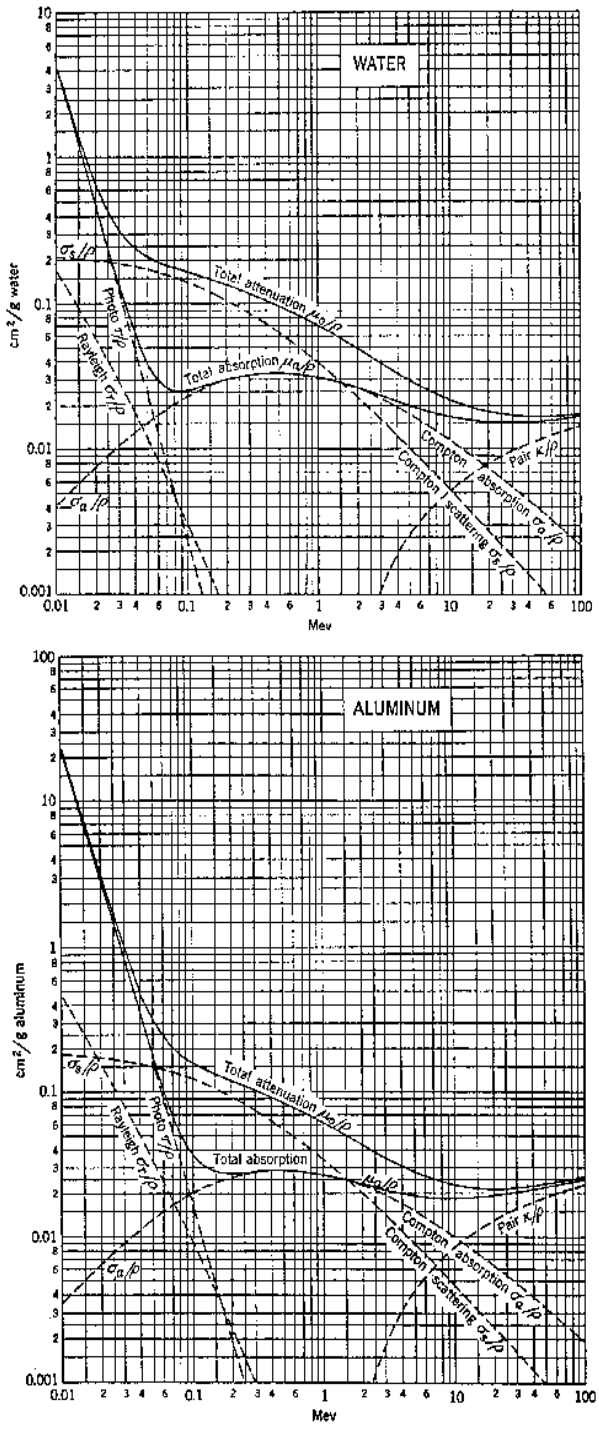
WATER
cm²/g water
Mev
Total attenuation μa/ρ
Total absorption μ/ρ
Photo τ/ρ
Rayleigh σr/ρ
Pair κ/ρ
Compton absorption σa/ρ
Compton scattering σs/ρ
ALUMINUM
cm²/g aluminum
Mev
Total attenuation μa/ρ
Total absorption
Photo τ/ρ
Rayleigh σr/ρ
Pair κ/ρ
Compton absorption σa/ρ
Compton scattering σs/ρ

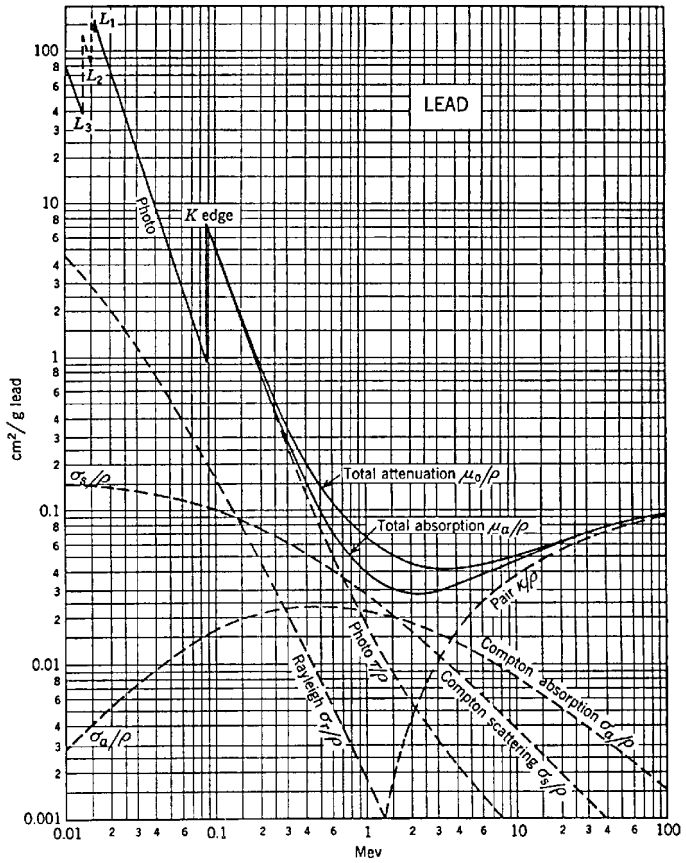

FIG. 6.17. Total and partial mass absorption and attenuation coefficients for γ-rays in water, aluminum and lead. (From R. D. Evans.)

$$E_e = E_\gamma - E_{be} \tag{6.23}$$

If the photoelectron originates from an inner electronic orbital, an electron from a higher orbital moves to fill the vacancy. The difference in binding energy of the higher and the lower energy orbital causes emission of X-rays and of low energy *Auger electrons*. The process of electron cascade, accompanied by X-ray and Auger electron emission, continues until the atom is reduced to its ground state energy. The photoelectron as well as the Auger electrons and the X-rays cause extensive secondary ionization by interacting with the absorber atoms.

The probability for the photoelectric effect decreases with increasing γ-ray energy. It is largest for the most tightly bound electrons and thus the absorption coefficient for the photoelectric effect increases in the order of electron shells K > L > M >, etc. In Figure 6.17 we see that in lead it is the dominating mode of absorption up to about 0.7 MeV. Discontinuities observed in the graph of μ vs E_γ are related to the differences in binding energies of the electrons in the different shells as the increasing γ-ray energy allows more

tightly bound electrons to be emitted. These discontinuities coincide with the K, L, etc., edges observed in X-ray absorption.

Gamma-rays of higher energy, rather than interacting with the field of the whole atom as in the photoelectric effect, interact with the field of one electron directly. This mode of interaction is called the *Compton effect* after its discoverer, A. H. Compton. In the Compton effect an electron is ejected from an atom while the γ-ray is deflected with a lower energy. The energy of the scattered γ-ray, E_γ', is expressed by the equation

$$E_\gamma' = E_\gamma - E_e \tag{6.24}$$

where E_e is the kinetic energy of the Compton electron. The probability for Compton scattering increases with target Z and decreases with E_γ. Since the Compton interaction occurs only with the most weakly bound electrons and high energy γ-rays, the binding energy of the electron is negligible compared to E_γ. The Compton electrons and scattered γ-rays have angles and energies which can be calculated from the relationships between the conservation of energy and momentum, correcting for the relativistic mass of the electrons at these kinetic energies. The scattered γ-ray may still have sufficient energy to interact further by the Compton effect, the photoelectric effect or pair production. Again, emission of X-rays and Auger electrons usually accompanies Compton interaction and extensive secondary ionization follows. Since the Compton electron can have a spread of values, the scattered γ-rays exhibit a broad spectrum. The Compton electrons, as in the case of photoelectrons, are eventually stopped by the processes described for β-particles.

Figure 6.17 shows the division of energy between the scattered Compton γ and the Compton electron as a function of γ-ray energy. Only the energy of the electron is deposited in the absorber as the scattered γ-ray has a high probability of escape. Thus Compton electrons contribute to the (*energy*) *absorption coefficient* μ_a while the Compton γ contributes to the *total attenuation coefficient* μ through the scattering coefficient μ_s in (6.9).

The fourth mode of interaction for γ-rays with an absorber involves conversion in the Coulomb field of the nucleus of a γ-ray into an electron and a positron (Fig. 6.18). This process is termed *pair production* since a pair of electrons, one positive and one negative, is produced. The process can be considered as the inverse phenomenon of positron annihilation. Since the rest mass of an electron corresponds to 0.51 MeV, the γ-ray must have a minimum value of 1.02 MeV to interact by pair production. As the energy of the γ-ray is increased beyond this value, the probability of pair production increases (see Fig. 6.17, where μ_{pair} is denoted). The excess energy (above the 1.02 MeV) appears as the kinetic energy of the electron pair.

$$E_\gamma = 1.02 + E_{e^-} + E_{e^+} \tag{6.25}$$

The pair of electrons are absorbed as described in §6.4. The annihilation of positrons produce 0.51 MeV γ's, which are absorbed by the processes described previously.

Figure 6.19 summarizes the domains of interaction of the main γ-ray absorption processes as a function of γ-ray energy and absorber Z-value.

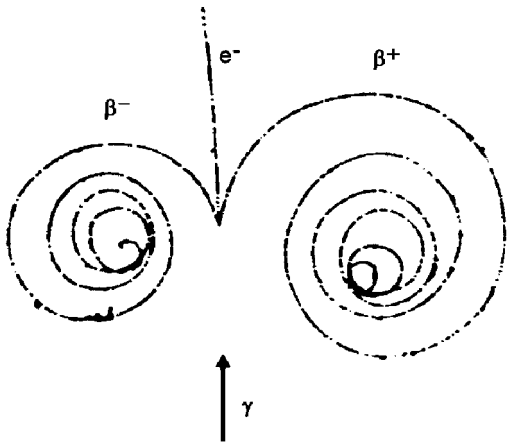

FIG. 6.18. Tracks of electron pair in a H_2 bubble chamber in a strong magnetic field perpendicular to the plane of the tracks. (Courtesy Lawrence Radiation Laboratory.)

6.6. Absorption of neutrons

A beam of collimated neutrons is attenuated in a thin absorber through scattering and absorption processes in a similar manner to the attenuation of γ-rays; these processes are described in previous §'s. In a thick absorber the neutrons are slowed from incident energy at the absorber face to thermal energies if the absorber is thick enough. The ultimate fate of the neutron is capture by an absorber atom. Because of the spread in neutron energy and the energy dependency of the capture cross-sections, no simple relation can be given for the attenuation of the neutron beam (cf. next section).

6.7. Radiation shielding

The absorption properties of nuclear radiation in material must be known in order to design shielding to avoid unwanted radiation effects on the surroundings by nuclear radiation sources.

For charged particles the shielding is usually slightly thicker than that required for the maximum range of projectiles in the material. Absorption thicknesses of 0.2 mm are adequate to completely absorb the particles from α-decay. By contrast 15 mm of materials of low Z such as water, plastic, etc., are required for absorption of β-radiation with energies up to 3 MeV. Radiation shielding constructed from materials of higher atomic number require correspondingly thinner thicknesses. The data in Table 6.2 and the curves in Figs. 6.6 and 6.13 provide information on the thickness of absorber material required for the energy of various types of radiation.

Since γ-rays and neutrons have no definite range but exhibit a logarithmic relation between thickness and intensity, only a partial reduction of the radiation can be obtained. Combining (6.6) and (6.7)

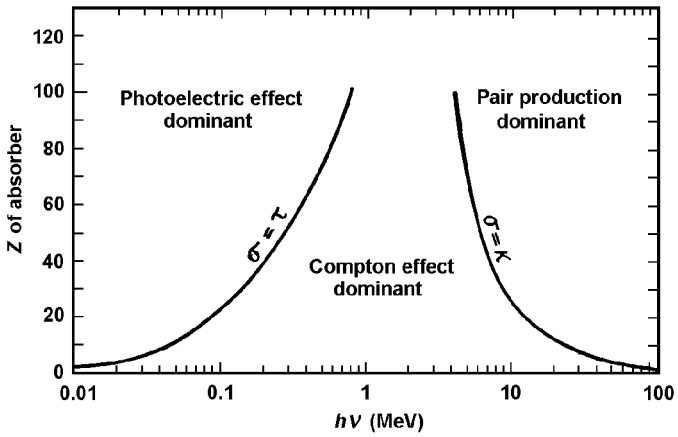

FIG. 6.19. Dominance regions for the three γ-ray absorption processes.

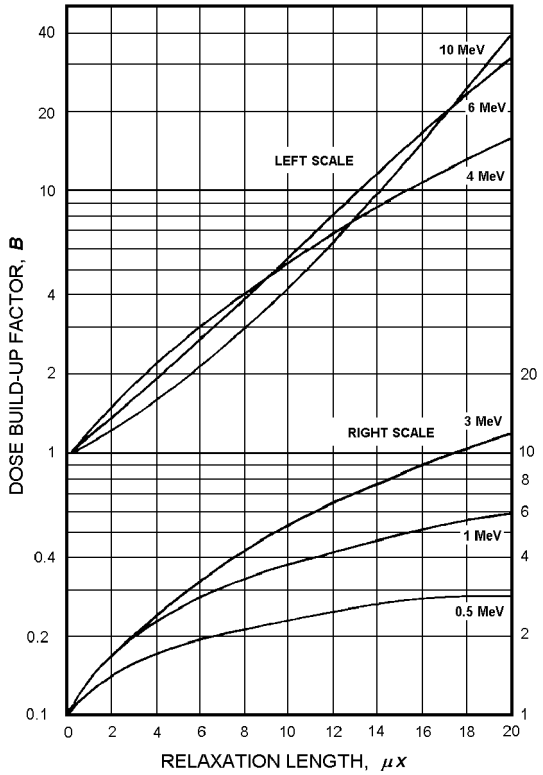

FIG. 6.20. Dose build-up factors in lead for a point isotropic source. Upper curves have scale to the left, lower curves to the right. (From *Radiological Health Handbook*.)

$$\phi = (nA/(4\pi r^2))e^{-\mu x} \tag{6.26}$$

it is seen that the intensity from a point source of radiation can be decreased by increasing either the distance from the source *r* or the thickness *x* of the absorber. Alternately, an absorber with a higher absorption coefficient, μ, can be chosen to reduce the thickness required.

Equation (6.26) is valid only for point sources with ideal geometry, i.e. no back or multiple scattering, etc. For γ-radiation the thicker the absorber the higher is the percentage of radiation which may be scattered backwards through secondary (mainly Compton) scattering. The effect of geometry and absorber thickness can be taken into account by including a constant *B* in the absorption equation:

$$\phi = B\phi_0 e^{-\mu x} \tag{6.27}$$

The "*dose build-up*" *factor B* not only takes into account multiple Compton and Rayleigh scattering but also includes correction for positron formation at high γ-energies and subsequent annihilation. Since for thick radiation shielding and high γ-energies the factor *B* may reach several powers of 10, it is quite important to be considered in designing biological shielding for radiation. Calculation of *B* is difficult and empirical data are most commonly used. Figure 6.20 gives *B*-values for a lead shield. The thickness of the shielding is given in relaxation lengths μ*x*. This value is obtained from diagrams like Figure 6.17; e.g. for a 3 MeV γ, μ_m is found to be 0.046 $cm^2\ g^{-1}$. If the absorber is 0.1 m thick the linear density is $10\rho_{Pb} = 113\ g\ cm^{-2}$ and the relaxation length becomes 5.2. With Figure 6.20 this gives (for the 3 MeV γ-line) a dose build-up factor *B* of 3. Thus the lead shield transmits three times more radiation than is expected by the simple relation (6.26). The flux reduction values for concrete and lead shielding in Figure 6.15 have been adjusted to take the dose build-up into consideration.

Equation (6.27) is not directly applicable for neutrons. For an estimate of required shielding we can use diagrams like that in Figure 6.21, which shows the attenuation of neutrons of three different energies in concrete and water, the most common neutron-shielding materials. It is necessary also to take into account the γ-rays emitted in neutron capture, which increases the shielding thickness required.

6.8. Analytical applications of radiation absorption

In previous sections of this chapter we have shown how different particles emitted in nuclear reactions are stopped in matter without causing nuclear reactions (nuclear reactions are treated later in this book). If the property of the particle is well defined (e.g. mass, charge, energy, etc) its interaction with the absorbing material can be well predicted, provided the composition of the absorbing material also is well defined. Conversely, the composition of the absorbing material (a "sample") can be determined from studying the absorption process (the "irradiation"). For example, atoms of the absorber (sample) may be knocked out and can be collected for analyses. When electrons are knocked out from the atomic shells of the absorber (sample) atoms, either the energy of these electrons may be analyzed, or the energy of the electromagnetic radiation emitted when the shells are refilled.

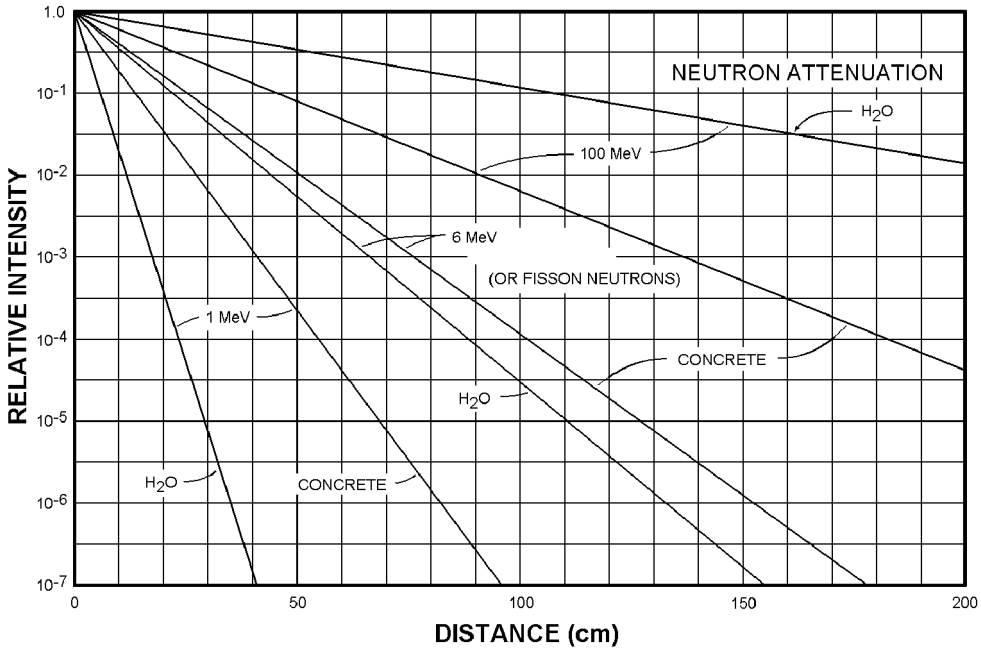

FIG. 6.21. Shielding thickness necessary to reduce a neutron beam in water and concrete. The 6 MeV lines can be used for fission neutrons. (From *Nuclear Data Tables*.)

These energies are characteristic of the sample and can thus be used for its identification. There are many analytical applications based on these principles, the most important ones will described in this Section.

6.8.1. *SIMS (Secondary Ion Mass Spectrometry)*

When heavy ions of energy largely exceeding the chemical binding energies, but with energies much lower than needed to cause nuclear reactions, hit a surface then atoms of this surface are *sputtered* out. These atoms, or actually ions, can be introduced in a mass spectrometer to determine the exact masses and mass/charge ratios, from which the element is identified. This is the bases for the SIMS analytical method for studying surfaces, particulary semiconductor surfaces. By bombarding with O^{2+} or Cs^{+} of ≤ 10 keV most surface elements can be detected (in fortunate cases down to the ppb range) with a resolution of the order 100 – 200 Å.

6.8.2. *PIXE (Proton or Particle Induced X-ray Emission)*

In the PIXE technique high energy protons (or heavier ions) are used to irradiate a thin sample (say 0.1 mg/cm^2). The probability for expulsion of an electron followed by the

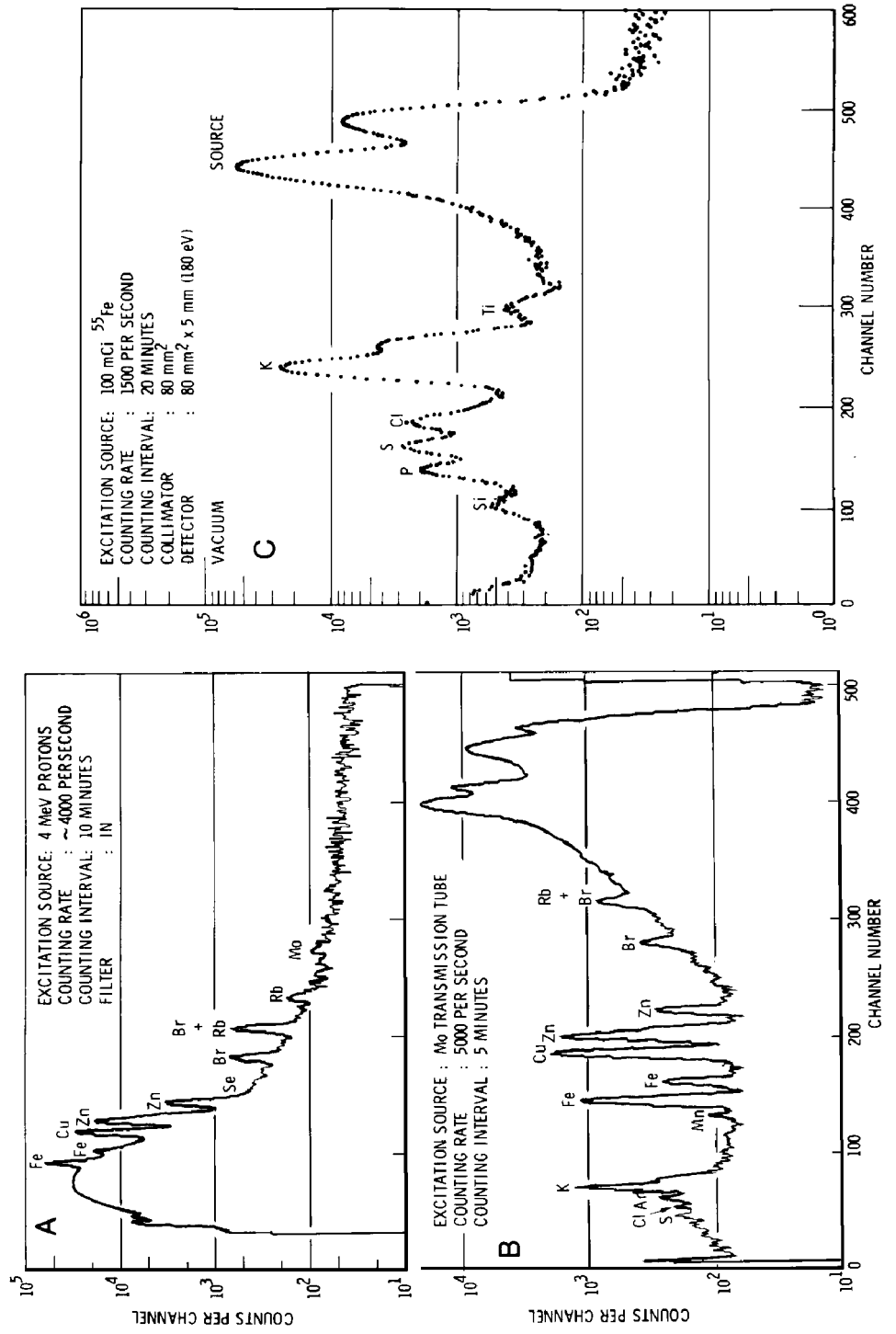

FIG. 6.22. PIXE analysis of trace elements in environmental and biological samples.

emission of a K-x-ray decreases with increasing Z of the sample; e.g. for 5 MeV protons the reaction cross section is ca. 10^{-25} m^2 for Z = 10 to 20 and about 10^{-28} m^2 (1 *barn*) for Z = 50; cf. Table 6.1. It can be shown that the reaction probability has a maximum when the incident particle has a velocity equal to the Bohr orbital velocity of the electron. Though the sensitivity decreases with Z elements up to Pb can be determined. The technique has primarily been used to determine trace elements in environmental and biological samples, see Figure 6.22(a).

6.8.3. *ESCA (Electron spectrometry for chemical analysis)*

High resolution β-spectroscopy can be used to determine chemical properties. A sample is irradiated with mono-energetic photons of $E_{\mathbf{h}}$, leading to the emission from the sample surface of photoelectrons. The relevant equation is

$$E_{\mathbf{h}} = E_{\mathrm{be}}(\mathrm{X,Y}) + E_{\mathrm{e}} \qquad (6.28)$$

where E_{e} is the kinetic energy of the emitted electrons, which can be determined very accurately (presently to about 0.01 eV) in the magnetic spectrograph; *photoelectron spectroscopy*. This sensitivity is much greater than chemical binding energies, E_{be}(X,Y), where X refers to an atom in compound Y. The probability for ejection of photoelectrons increases with decreasing photon energy (Fig. 6.16 and 6.19) and therefore low energy X-rays are used as a source.

Although it is the outermost (or most weakly bound) electrons which form the valency orbitals of a compound, this does not leave the inner orbitals unaffected. An outer electron (which we may refer to as e_L) of an atom X_1 which takes part in bond formation with another atom X_2 decreases its potential, which makes the inner electrons (which we may call e_K) more strongly bound to X_1. Thus $E_{\mathrm{be}}(e_K)$ increases by an amount depending on $E_{\mathrm{be}}(e_L)$. Although this is a somewhat simplified picture, it leads to the practical consequence that the binding energy of e_K, which may be in the 100 – 1000 eV range, depends on the chemical bond even if its orbital is not involved directly in the bond formation. Figure 6.23 shows the ESCA spectrum of trifluoroacetate. Since the largest chemical shift, relative to elementary carbon, is obtained for the most electronegative atoms, the peaks refer to the carbon atoms in the same order as shown in the structure.

6.8.4. *XFS (X-ray fluorescence analysis)*

If a sample containing atoms of a particular element (e.g. Ag) is irradiated with photons of energy high enough to excite an inner electron orbital (e.g. the K_α orbital in Ag at 22.1 keV), X-rays are emitted in the de-excitation. If the photon source is an X-ray tube with a target made of some element (Ag in our example), the probability is very high that the K_α X-ray emitted from the source would be absorbed by the sample atoms and re-emitted (*fluorescence*). (This is an "electron shell resonance absorption" corresponding to the Mössbauer effect, although the width of the X-ray line is so large that recoil effects can be neglected.) The spectrum of the scattered X-radiation (or, more correctly, photon radiation

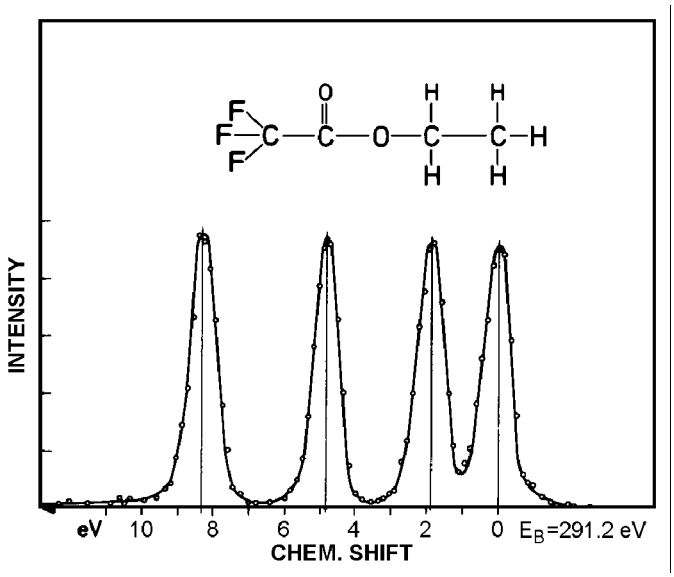

FIG. 6.23. ESCA spectrum of trifluoroacetate.

emitted from the sample) is referred to as the *X-ray fluorescence spectrum*. It contains lower energy radiation including K_α radiation emitted by atoms of lower atomic number. The height of these other peaks is lower because of a lower reaction cross-section (Fig. 6.24). Figure 6.22(B) illustrates an XFS analysis of a biological sample.

X-ray fluorescence analysis using vacuum tube sources have become a well-established analytical technique in the last decade. Nuclear interest stems partly from the possibility of using radioactive sources for stimulating X-ray fluorescence in a sample. These sources can be classified depending on the mode of production of the X-rays:

(i) γ-ray sources: decay between closely located nuclear energy levels, e.g. a 59.5 keV γ emitted in the α-decay of ^{241}Am: also "broad spectrum" γ-sources like ^{125}I are used.

(ii) x-ray sources: (a) radiation emitted in rearrangement of electron orbitals following α- or β-decay (primary X-rays), e.g. 11.6-21.7 keV uranium L-X-rays from ^{238}U formed in the α-decay of ^{242}Pu, or 41.3-47.3 keV europium K-X-rays from β-decay of ^{153}Gd; (b) irradiation of a target with α-, β-, or γ-radiation leading to ionization and excitation of the target atoms and its de-excitation by X-ray emission.

(iii) Bremsstrahlung sources, e.g. T in titanium, or ^{147}Pm in aluminum (Fig. 6.10).

An important advantage of radioactive X-ray fluorescence sources is that very small instruments requiring no (X-ray) high voltage or current can be designed for field applications. Such instruments are used in geological investigations (bore holes, mineral samples, etc.), in-line mineral analysis (Zn, Cu, and other ores in flotation cycles, Ca in cement raw-material, etc.), on-line analysis of surface depositions (Zn on iron sheets, Ag in photographic emulsions, etc.). Figure 6.22 shows fluorescent spectra obtained on bovine liver with three different excitation sources: (A) 4 MeV protons (PIXE), (B) (conventional) molybdenum transmission tube, and (C) radioactive ^{55}Fe.

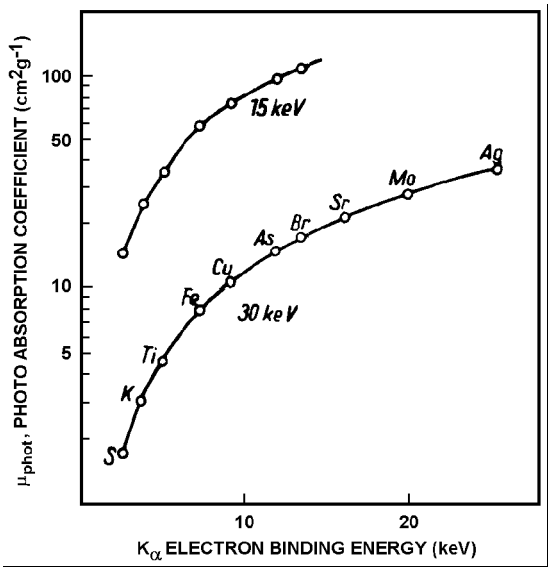

FIG. 6.24. Photoelectron absorption coefficients at K_α edges for 10 and 30 keV γ-rays as function of absorber material. The photo effect is the dominating absorption mode.

6.8.5. *Mössbauer effect*

According to the wave model of the atom, electrons in the innermost orbitals have a finite probability of existence within the nucleus. These electrons interact with the nuclear charge distribution, and thereby affect the nuclear energy levels (cf. §11.3.3). The extent of the effect depends on the exact properties of the electron orbitals involved, which vary with different chemical compounds. Therefore a γ-ray emitted from an isomeric state of an atom bound in one chemical compound may have a slightly different energy than from the same atom bound in another compound. This difference, referred to as the *isomer* (*energy*) *shift*, is extremely small, only about 10^{-10} of the energy of the emitted γ. Nevertheless, it can be measured by a technique developed by R. Mössbauer. The fundamental physics involved and technique used is well illustrated by Mössbauer's original experiment. Mössbauer placed an ^{191}Os source about a half-meter from a γ-ray detector A as shown in Figure 6.25. An iridium foil absorber was placed between the source and detector so that some of the photons of 129 keV energy from the ^{191}Os were absorbed by the iridium atoms in the foil, exciting these atoms from the ground state (3/2 +) to the 5/2 + state. Because of the short half-life of the latter state it immediately decayed, re-emitting the γ-ray. The emission was isotropic, i.e., occurs in all directions. The result was a reduction in intensity measured by detector A but an increase in the count rate in detector B.

The conditions for such a *nuclear resonance absorption* are very stringent. Using the Heisenberg relationship (4.66) we can estimate the half-value width of the 129 keV peak to be 5×10^{-6} eV. We can also use relation (4.34) to calculate the iridium atom recoil energy to be 46×10^{-3} eV. Thus the γ-ray leaves the source with an energy of (129×10^3

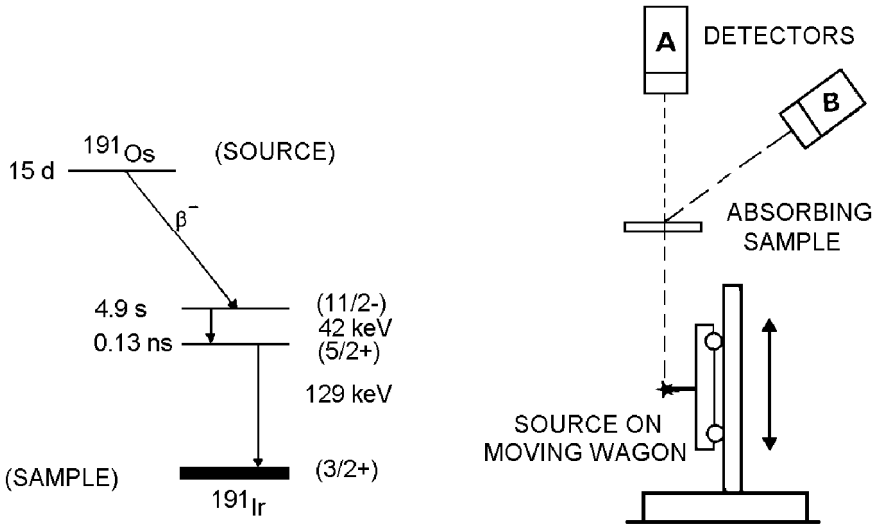

FIG. 6.25. Decay scheme of ^{191}Os and principle of a Mössbauer experiment.

– 46 × 10^{-3} eV). Also, in order for the 129 keV γ-ray to be absorbed in ^{191}Ir, it must arrive with an excess energy of 46 × 10^{-3} eV to provide for the conservation of momentum of the absorbing atom. Thus there is a deficit of 2 × 46 × 10^{-3} eV, which is very different from the value of the very narrow energy width of the γ-ray. Consequently, no resonance absorption can take place.

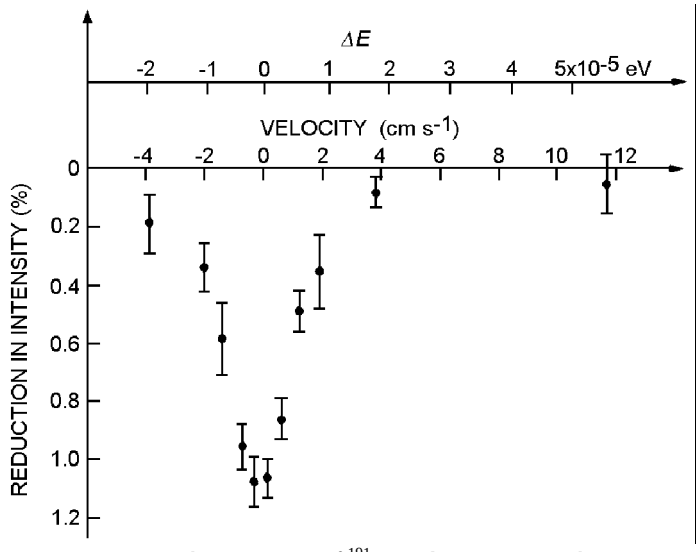

FIG. 6.26. Mössbauer spectrum of ^{191}Ir metal. (From R. Mössbauer.)

The limitation posed by the recoil phenomenon can be circumvented. If the source and absorber atoms are fixed in a crystal, the recoil energy may be insufficient to cause bond breakage. The energy is absorbed as an atomic vibration in the crystal, provided the quantization of the vibrational states agree exactly with the recoil energy. If not, which is often the case, the absorber atom stays rigid in the lattice, and the recoil energy is taken up by the whole crystal. In this case it is necessary to use the mass of the crystal in (4.34) rather than the mass of a single atom. Under these circumstances the recoil energy becomes infinitesimally small for the emitting as well as the absorbing atom; this is called *recoilless absorption*. The probability for recoilless absorption is improved if the source and absorber are cooled to low temperatures.

The data of Figure 6.26 were obtained by recoilless absorption in osmium metal containing ^{191}Os (source) and Ir metal, both cooled in cryostats. By slowly moving the source (with velocity v) towards or away from the absorber (see Fig. 6.25), some kinetic energy E_γ is added or subtracted from the source energy E_γ as "detected" by the absorber (Doppler effect). The energy and velocity relationship is given by the Doppler equation

$$E_\gamma / E_\gamma = v/\mathbf{c} \tag{6.29}$$

The velocity is shown in the Figure, where a value of v of 1 cm s^{-1} corresponds to 4.3×10^{-6} eV. The half-value of the γ-peak is found to be about 20×10^{-6} eV, i.e. a factor 4 times higher than calculated by the Heisenberg relationship. This is due to Doppler broadening of the peak as a consequence of some small atomic vibrations. Although the Mössbauer method can be used for measurements of γ-line widths, the results are subject to considerable errors.

One of the most striking uses of the extreme energy resolution obtainable by the Mössbauer effect was achieved by R. V. Pound and G. A. Rebka, who measured the emission of photons in the direction towards the earth's center, and in the opposite direction from the earth's center. They found that the photon increased its energy by one part in 10^{16} per meter when falling in the earth's gravitational field. This can be taken as a proof that the photon of $E_{\mathbf{h}} > 0$ does have a mass.

When a "Mössbauer pair" (like ^{191}Os/Ir, or ^{57}Co/Fe, ^{119m}Sn/Sn, ^{169}Er/Tm, etc.) have source and absorber in different chemical states, the nuclear energy levels differ for the two Mössbauer atoms by some amount E_γ. By using the same technique as in Figure 6.25, resonance absorption can be brought about by moving the source with a velocity corresponding to E_γ. In this manner, a characteristic *Mössbauer spectrum* of the compound (relative to a reference compound) is obtained; the location of the peaks (i.e. the absorption maxima) with respect to a non-moving source (the *isomer shift*) is usually given in mm s^{-1}.

Figure 6.27 shows the isomer shifts obtained for a number of actinide compounds. The positions of the isomer shifts show the effect of valence states due to different population of the 5f orbitals. The different shifts for compounds of the same valence state is a measure of the variation in the covalency of the bonding. The compounds on the left are metallic. The shifts reflects the contributions of conduction electrons to the electron density at the nucleus of neptunium.

Mössbauer spectroscopy is limited to the availability of suitable sources. About 70 Mössbauer pairs are now available. The technique provides a useful method for studying

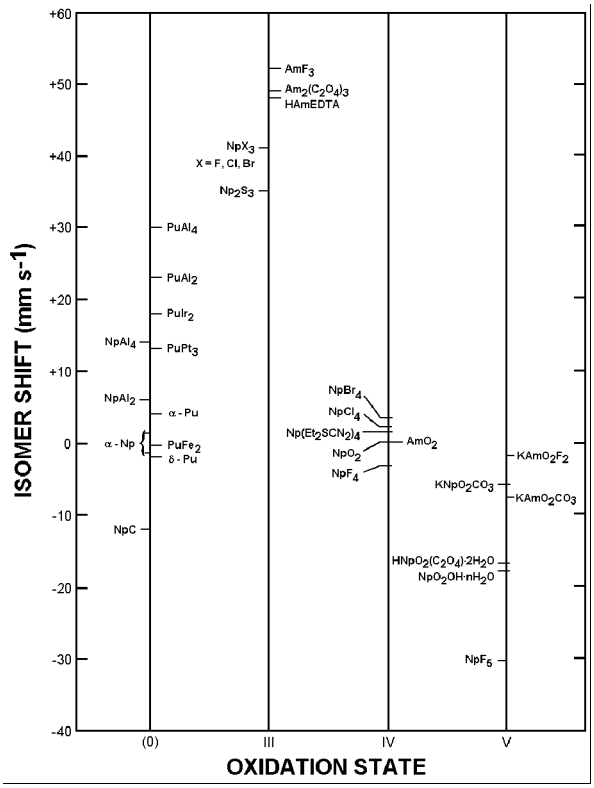

FIG. 6.27. Isomer shifts for some actinide metals and actinide compounds.

chemical compounds in the solid state, especially compounds which are nontransparent to light and chemically or radioactively unstable.

6.9. Technical applications of radiation sources

Nuclear radiation absorption methods have many technical applications. These methods are not to be confused with radioisotope tracer methods, although radioisotopes may be used as radiation sources. In the tracer method the chemical properties of the radionuclide are important while in the applications discussed in this section only the type and energy of radiation emitted are important.

As a *source* of radiation in such technical applications, either accelerators or radiation from radionuclides can be used. Interchangeable radionuclides have the advantage over accelerators as radiation sources in that they can cover a larger energy range from high energy γ-rays to low energy β-rays in a much simpler way. This makes it possible to select the type and energy of radiation which have the most advantageous properties for a particular use. An additional advantage of radionuclides is that the sources can usually be made much smaller than X-ray sources, enabling them to be used in places where larger equipment is inconvenient or impossible to place. The fact that radionuclides require neither

electric power nor cooling also renders them more suitable for field applications. Further, their independence from effects of temperature, pressure, and many other factors results in higher reliability compared to X-ray generators. Finally, and, perhaps as important as any of the other factors, they are in general much less expensive than accelerators.

To counterbalance these advantages is the disadvantage of the inability to turn off the radiation from radionuclides. This often requires that the radiation source be well shielded, adding to its weight and cost. An additional drawback to the use of radionuclides is that they have to be replaced after a few half-lives. The seriousness of this disadvantage depends upon the lifetime of the particular nuclide and is unimportant in cases where longlived sources can be used.

The extensive use of radionuclides in industry is illustrated by Table 6.3, which summarizes the various studies undertaken by I.C.I., UK, in "a typical year".

6.9.1. *Radionuclide gauges*

Radionuclide gauges are a measurement system consisting of two parts, a radioactive source and a detector, fixed in some geometry to each other. They are used mainly for control in industrial processes but can also be applied for specific analyses. The gauges come in two types. In one type the radiation source and the detector are on opposite sides of the technical arrangement to be measured; these are known as transmission or absorption instruments. In the second type, known as reflection or back-scattering instruments, the radiation source and the detector are on the same side. The instruments are also classified with respect to the kind of radiation involved. For example, γ-transmission, β-reflection, secondary X-ray instruments, etc. These radioisotope gauges are used for measurements of thicknesses, densities, etc.

TABLE 6.3. *Radioisotope based studies undertaken annually by a large chemical company*

Technique[a]	Number of applications
Level and interface measurements:	
γ-ray absorption	210
Neutron backscatter	480
γ-ray backscatter (storage cavities)	71
Blockage detection and deposition:	
γ-ray absorption	132
Neutron backscatter	129
Entrainment and voidage:	
γ-ray absorption	86
Thickness and corrosion measurements	15
Distillation column scans	108
Flow measurements:	
Pulse velocity	483
Dilution techniques	84
Leak detection	90
Residence-time studies	21
Carry-over studies (tracer)	6

[a] Less commonly used techniques have not been included.

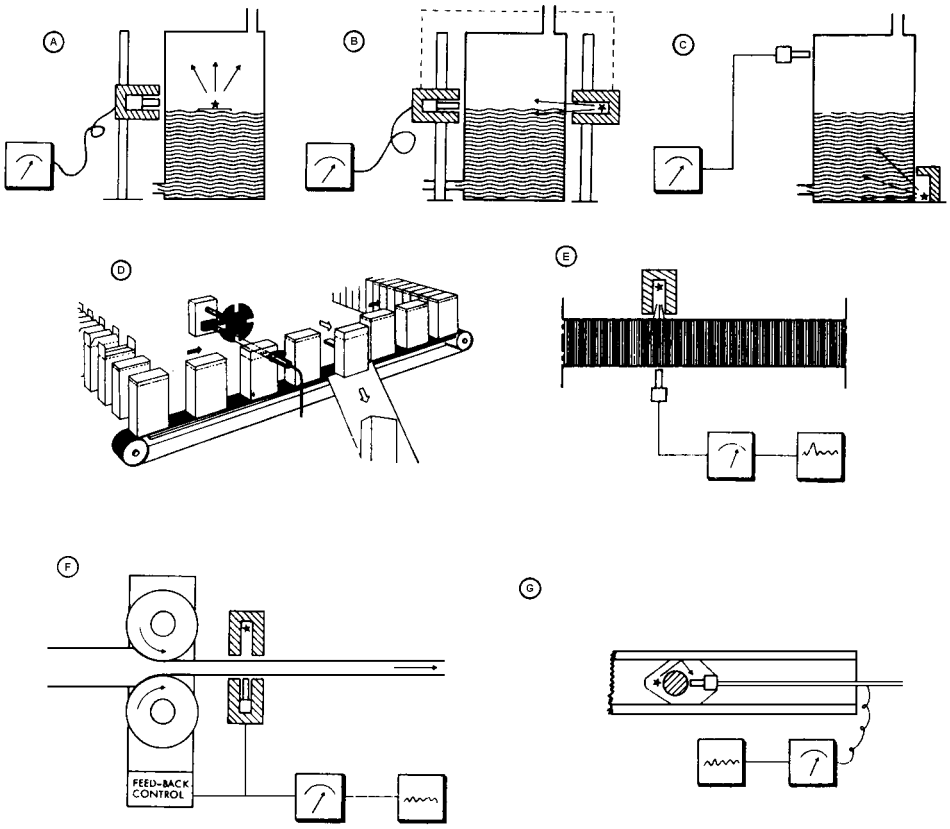

FIG. 6.28. Radionuclide gauges for: A-C level measurements in tanks, D control of package filling, E flow density measurements, F thickness control, and G wall material in pipes and bore holes.

In Figure 6.28 a number of types of application for transmission instruments are illustrated. Illustrations A–C show measurements of level control. Type A can be used only for liquids while B and C can be used for all kinds of material. The latter instruments are uniquely suitable for application to large storage containers for grain, wood chips, oil, sand, cement, etc., and for material under extreme conditions such as molten glass and metal, explosives, etc. Level gauges are also used in the control of the filling or packages, cans, etc. in industry as illustrated in D.

Let us consider a somewhat unusual application of this type of instrument. In the manufacture of titanium it is important to keep liquid $TiCl_4$ at a particular high temperature and pressure in a vessel. $TiCl_4$ has a triple point (i.e. the pressure and temperature conditions at which all three phases - solid, liquid, and vapor - of a substance are at equilibrium) in the neighborhood of the particular technical conditions. By using a γ-density gauge it is possible to detect when the triple point is exceeded because of the disappearance of the vapor-liquid interface. This allows a simple method of control of the process conditions in the vessel.

The use of radioisotope gauges in density measurements is dependent upon (6.26) in which *r* and *x* are constant while the absorption coefficient is density dependent (i.e. dependent on the average atomic composition of the absorber). A practical arrangement is illustrated in Figure 6.28, E, where the density of a medium in a pipeline is measured. This medium may be a mixture of gas and liquid such as water and water liquids with different composition and different amounts of dissolved substances as, for example, oil, salts or acids in water, process solutions in general or sludges, and emulsions such as fruit juices, latex emulsions, etc. From the variation in density the concentration and composition may be determined. Such density gauges are also used for control in filling of soft drink bottles and cans and submerged in rivers and lakes for measuring the depth of the bottom silt, etc. Density gauges are used in the production and the fabrication of such diverse products as automobile tires and cigarette packages.

Thickness gauges are the most common type of instrument using the absorption technique. In this case *x* in (6.26) is varied. Measurements can be carried out on all kinds of materials with thicknesses of ≤ 100 g cm^{-2} and is independent of the temperature and of whether the material is stationary or in motion. Figure 6.29, F, illustrates the application of a thickness gauge in a rolling mill where material of constant thickness is produced by using the signal from the detector for control purposes. Thickness gauges are used in the fabrication of glass, metal, paper, plastic, rubber, candy bars, etc. They have been used for measuring the thickness of snow in polar regions, icing on airplane wings, and other applications in which it is necessary to use remote operation.

In order to measure very thin layers of material such as coatings of paint, wax, and plastic films on papers or other material, two thickness gauges are used with a differential coupling so that one detector measures the uncovered and the other the covered or treated portion of the material. Thickness gauges also are used in industry to measure the degree of wear in industrial machinery. For surface measurements of thicknesses ≤ 0.8 g cm^{-2} most thickness gauges use radiation sources with β-emitters while for thicknesses of 0.8–5 g cm^{-2} bremsstrahlung radiation sources are most suitable. For even thicker materials γ-emitters are used.

Use of reflection gauges depends on the fact that the intensity of the scattered radiation under conditions of constant geometry depends on the thickness of the scattering material and its electron density (if β- or γ-sources are used). If neutrons are used the mass number of the scattering material is of prime importance. The electron density of the scattering material varies with the particular element and the chemical composition. Frequently, it is possible to determine the thickness and the nature of a surface layer by means of β-scattering. Reflection gauges have been applied to on-line analysis of tin-covered iron plates, metal coatings on plastics, paint layers, and to measuring the protective coating inside pipelines (Fig. 6.29, G). In some instances γ-radiation sources are preferred over β-emitters in measurements of material with greater wall thicknesses, particularly when transmission measurements are not feasible. Steel thickness from 1 to 20 cm has been measured with 5% accuracy using backscattering from ^{60}Co or ^{137}Cs sources of 20 μCi intensity.

Scattering and reflection are dependent on the electron density of the absorber, which is approximately proportional to the value of Z/A. Backscattering of β-particles from organic compounds is therefore very dependent on the hydrogen concentration ($Z/A = 1$) but fairly independent of the concentration of C, N, and O ($Z/A = 0.5$). This has led to the development of sensitive instruments for hydrogen analysis for various organic and

water-containing materials. In an instrument using 10 mCi ^{90}Sr, the hydrogen concentration in a 10 ml sample can be determined in 20 min with 0.03% accuracy. This is not only superior to other conventional analytical methods, it also has the advantage of being a nondestructive technique.

Neutrons are slowed down most effectively by light elements (§12.6). As a consequence, neutron scattering can be used for the analyses of light elements, particularly hydrogen. In one type of instrument the radiation source consists of ^{252}Cf which produces fast neutrons (from spontaneous fission), while the detector is sensitive only to slow neutrons. This system is used for studies of ground water and analysis of bore holes in wells (Fig. 6.29, G). These analyses are usually combined with density determinations using a γ-source, thereby making it possible to identify strata of water, oil, coal, etc.

Some properties and uses of commercial radionuclide gauges are listed in Table 6.4.

6.9.2. *Radiography*

Radiography is a photographic technique in which nuclear radiation is used instead of light. Medical examination and nondestructive industrial testing using X-rays generated by high-vacuum tubes are the most important areas. A number of suitable sources of radioactive nuclides for producing radiograms are given in Table 6.4.

Beta-radiography is only suitable for thin objects and not widely applied. On the other hand, γ-radiography is a common nondestructive test technique in which normally ^{137}Cs or ^{60}Co has been used. γ-radiography has advantages in field use and in detection of sensitive objects. The radiation source can be ^{60}Co, which is normally kept in a portable radiation shielding of 30–60 kg of lead and situated at the end of a rod so that it can be pushed out of the shielding for use. The photographic film is located in a cassette surrounded by amplifying screens.

TABLE 6.4. *Some commercially available radionuclide gauges and γ-sources for radiography (France)*

Radiation	Source	$t_{½}$	Application
α	U or Ra	Long	Thickness control in manufacturing paper, aluminum; ≤ 60 g/m^2
Soft β	^{147}Pm(0.2 MeV)	2.6 y	Thickness control; ≤ 400 g/m^2
β, soft γ	^{204}Tl(0.8 MeV)	3.8 y	Thickness: 1.10 mm steel, 3-50 mm glass; 8-100 kg/m^2
Hard β	^{144}Ce(3 MeV)	0.78 y	Thickness ≤ 1 mm steel; ≤ 10 kg/m^2
X	^{109}Cd(88 keV)	1.24 y	Detection of S-content in hydrocarbons
n,γ	RaBe, ^{137}Cs	30 y	Moisture-density meter for civil engineering and agriculture
γ	^{60}Co(1.3 MeV)	5.3 y	4 MBq source for backscatter on ≤ 20 mm steel, 0.4 - 40 GBq for remote level indication
Soft γ	^{192}Ir(0.3 MeV)	74 d	400 GBq, 26 kg: ≤ 40 mm steel radiography
Medium γ	^{137}Cs(0.7 MeV)	30 y	400 GBq, 45 kg: ≤ 70 mm steel pipeline inspection
Hard γ	^{60}Co(1.3 MeV)	5.3 y	10 TBq, 900 kg: ≤ 180 mm steel radiography

The exposure *At* (GBq hours) required for an optical density (*D* = log (incident light/transmitted light)) ~ 2 at an absorber (object) thickness *x* (cm) using a typical industrial X-ray film and a ^{60}Co γ-ray source positioned at a distance of 1 m from the film can be estimated by the expressions

$$\log(At) = 1.068 + 0.135\,x \qquad \text{for an iron absorber}$$
$$\log(At) = 1.068 + 0.040\,x \qquad \text{for a concrete absorber}$$

Exercise 6.14 is an example of the use of these expressions.

Gamma-radiography has been used for determining the number of reinforced iron bars in concrete construction, cavities in various kinds of castings (as explosives, plastics or metals), cracks or other defects in turbine blades in airplane parts, detonators in unexploded bombs, welded joints in pressure vessels, distillation towers and pipes, corrosion inside pipes and furnaces, and medical field X-rays, to mention only a few applications. Gamma-radiography is used throughout the world for product control leading to improved working safety and economy.

Because γ-absorption occurs through interaction with the electrons, objects of high atomic numbers show the strongest absorption. By using neutrons instead of γ-rays, the opposite effect is achieved, i.e. low *Z* objects are most effective in removing neutrons from a beam. This is used in *neutron radiography* in which both reactor neutrons and neutrons from ^{252}Cf sources are applied. Because of the higher neutron flux from the reactor than from ^{252}Cf sources of normal size (i.e. ≤ 1 mg) the exposure time at the reactor is much shorter. On the other hand, the small size of the ^{252}Cf source offers other conveniences.

6.9.3. *Radionuclide power generators*

The absorption of radiation leads to an increase in the temperature of the absorber. An example of this is the absorption of the kinetic energy of fission products in nuclear reactor fuel elements which is a main source of the heat production in reactors. The absorption of decay energy of radioactive nuclides in appropriate absorbing material can be used in a similar - albeit more modest - way as an energy source.

Figure 6.29 shows the principles of two different radioisotope power generators, the larger (to the left) is of SNAP-7 type and produces ~ 60 W, the smaller one produces ~ 10 mW. The radiation source for the larger generator consists of 15 rods (A) clad with hastelloy and containing approximately 7 kg of $SrTiO_3$ which has approximately 225 000 Ci of ^{90}Sr. This heat source is surrounded by 120 pairs of lead telluride thermoelements (B) and a radiation shield of 8 cm of depleted uranium (C). The whole arrangement is surrounded by a steel cover with cooling fins. The weight of this generator is 2.3 t with dimensions of 0.85 m in length and 0.55 m in diameter. It is estimated that the lifetime of such an energy source is at least 5 y, although the half-life of ^{90}Sr (30 y) promises a longer period. Radionuclide generators in unmanned lighthouses, navigation buoys, automatic weather stations, etc., in sizes up to about 100 W, have been in use in a number of countries, e.g. Japan, Sweden, the UK, the USA, etc. Since no moving parts are involved, these generators need a minimum of service. Their reliability makes them valuable in remote areas like the Arctic regions where several such generators have been installed.

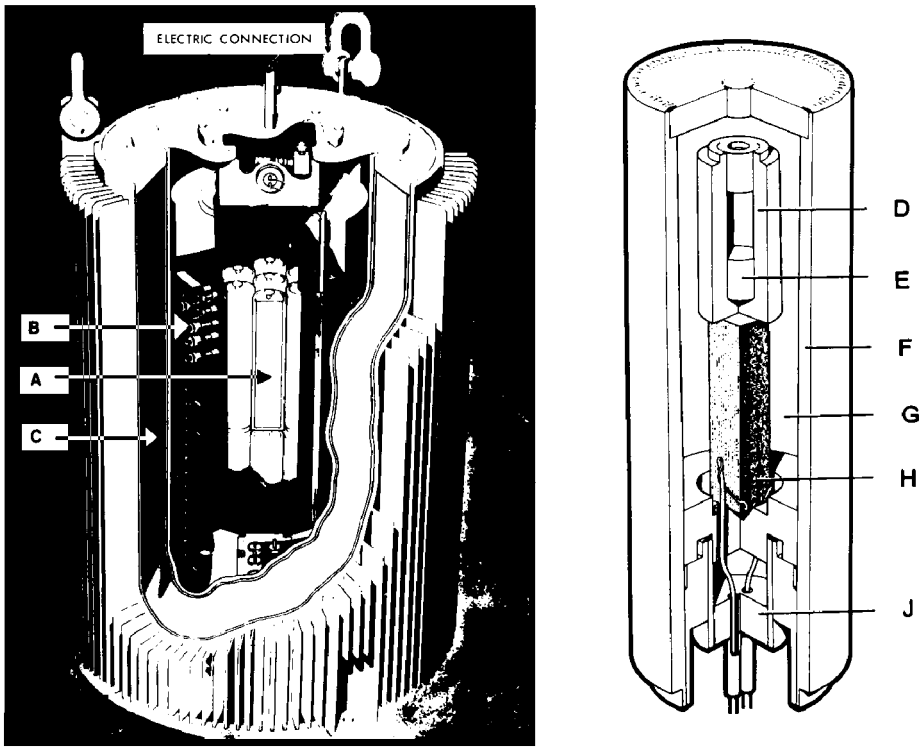

FIG. 6.29. A - $^{90}SrTiO_3$; B - thermocouples; C - radiation shield (depleted U); D - capsule; E - ^{238}Pu; F - secondary containment; G - thermal insulation; H - thermopile; J - insulator.

^{90}Sr is the preferred radionuclide for terrestrial uses. Its power density is relatively high, 0.93 W g^{-1}, as compared to some other possible radionuclides as ^{137}Cs (0.26 W g^{-1}) and ^{238}Pu (0.55 W g^{-1}), but it is lower than ^{244}Cm (2.8 W g^{-1}) and ^{245}Cm (121 W g^{-1}). Recently ^{60}Co has come into use; the heating mainly comes from absorption of the γ's in a uranium shielding.

^{238}Pu has been used as an energy source in space. Several satellites with radioisotope generators of 25 W have been placed in space, and the Apollo project employed a generator "SNAP-27" containing ^{238}Pu with a total weight of 14 kg and producing 50 W power. The Viking landers on the planet Mars used ^{238}Pu as the main energy source. It was used also to power the Pioneer vehicles which gave us the first close pictures of the planet Jupiter and in the Voyager missions to the outer planets (in August 1989 one of them passed Neptunus at ~ 5000 km altitude, taking remarkable close-up pictures) where the ^{238}Pu power source produced 450 W. One will reach the star Sirius in about 300 000 years!

6.10. Exercises

6.1. In §6.3 two equations are given for calculating the range of α-particles in air and in other material from the particle energy as well as a curve for the range in aluminum. How different are the values from the equations and from the curve for a 5 MeV α?

6.2. What is the minimum energy that an α-particle must have to be detected by a GM tube having a mica (the density is approximately equal to aluminum) window of 1.5 mg cm^{-2}?

6.3. For an irradiation experiment it is necessary to extract a beam of deuterons from an accelerator. The projectile energy is 22 MeV D^+. For this purpose the beam is deflected and permitted to pass through a thin titanium foil (density 4.5 g cm^{-3}). Assuming that $R_1\rho_1 M_1^{-1/2} = R_2\rho_2 M_2^{-1/2}$ (Bragg-Kleman rule), what is the maximum thickness of the foil? Give the answer in millimeters.

6.4. Make a rough estimate of the range in air for a 1 MeV α, 1 MeV H^+ and 1 MeV e^- using the plot in Fig. 6.7. The energy to form an ion pair in air is 14.6 eV but assume that twice as much energy is lost through excitation.

6.5. What is the range of a 6.3 MeV α-particle in (a) aluminum, (b) nickel, (c) platinum?

6.6. What is the γ-ray flux from a 3.7 GBq ^{60}Co source at a distance of 3 m? Assume $\psi_{sample} = 1$.

6.7. What is the maximum range in millimeters of β-particles from T, ^{14}C, ^{32}P and ^{90}Sr in a photographic emulsion if its absorption efficiency is assumed to be the same as aluminum? The density of the emulsion is assumed to be 1.5 g cm^{-3}.

6.8. The E_{max} of ^{32}P β-particles is 1.71 MeV. To what electron velocity does this correspond?

6.9. In a laboratory an irradiation area must be designed for γ-radiography using a 3.7×10^{11} Bq ^{60}Co source. For this purpose a cubic building is erected with an interior side length of 2 m. The desired flux reduction is 10^6. How thick must the wall be and how much will the shielding material cost (i.e. not including labor costs) if it is made of (a) concrete? (b) lead? Assume lead blocks cost $1.50 per kg and concrete $40 per m^3.

6.10. An experiment is done with ^{60m}Co which emits 0.05860 MeV γ. The detector used is a NaI crystal. What photo peaks will be observed if the electron binding energies in sodium are K 1072 and L 63 eV, and in iodine K 33 170 and L 4800 eV?

6.11. A human body may be considered as consisting of water. Radiation from ^{137}Cs is absorbed by a 15 cm thick body. How much is the γ-ray flux reduced by the body, and how much of the beam energy (β plus γ) is absorbed?

6.12. For iron the mass attenuation coefficients are: at 0.5 MeV γ, 0.083; at 1.0 MeV, 0.059; at 1.5 MeV, 0.047 cm^2 g^{-1}. Calculate the corresponding one-tenth values.

6.13. An absorption curve of a sample emitting β- and γ-rays was taken with aluminum absorber using a gas-flow proportional counter. The data obtained were:

Absorber thickness (g cm^{-2})	Activity (counts min^{-1})	Absorber thickness (g cm^{-2})	Activity (counts min^{-1})
0	5800	0.700	101
0.070	3500	0.800	100
0.130	2200	1.00	98
0.200	1300	2.00	92
0.300	600	4.00	80
0.400	280	7.00	65
0.500	120	10.00	53
0.600	103	14.00	40

(a) Estimate the maximum energy of the β-spectrum. (b) Find the energy of the γ-ray.

6.14. A 40-story high modern business building is supported by 0.9 m thick pillars of reinforced concrete. The insurance company must check that the number of iron bars are as many as required, and therefore they want to investigate the pillars by γ-radiography. What exposure times are required for (a) a small 200 GBq ^{60} Co source, (b) for a large 150 TBq source? Use the same film data as in 6.9.2.

6.15. A swimming-pool reactor produces a flux of 3×10^{16} thermal neutrons m^{-2} s^{-1} at 1 m from the reactor center. Assuming a parallel beam of neutrons diffusing up to the surface of the pool where the neutron flux is measured to be 10^8 n m^{-2} s^{-1}, calculate the thickness (x m) of the water layer required. For thermal neutrons the flux is reduced exponentially with the exponent $x\,L^{-1}$, where L is the diffusion length (2.75 cm in H_2O).

6.16. In a sample of 10.4 TBq of old fission products, the average γ-ray energy is 0.5 MeV and on the average 0.4 γ's are emitted per β-decay. (a) What is the lead shielding required to reduce the γ flux to 10^2 γ cm^{-2} s^{-1}

at 1.5 m from the source assuming only exponential absorption? (b) What is the relaxation length? (c) What is the build-up factor?

6.11. Literature

B. T. PRICE, C. C. HORTON, and K. T. SPINNEY, *Radiation Shielding*, Pergamon Press, Oxford, 1957.
S. FLÜGGE (ed.), *Handbuch der Physik*, Band 34, 1958, and 38/2, 1959, Springer-Verlag.
R. L. MÖSSBAUER, Recoilless nuclear resonance absorption, *Ann. Rev. Nucl. Sci.* **12** (1962) 1.
J. C. ROCKLEY, *An Introduction to Industrial Radiology*, Butterworths, London, 1964.
C. S. FADLEY, S. B. M. HAGSTRÖM, J. M. HOLLANDER, M. P. KLEIN, and D. A. SHIRLEY, Chemical bonding information from photoelectron spectroscopy, *Science* **157** (1967) 1571.
D. A. SHIRLEY, Chemical tools from nuclear physics, *Science* **161** (1968) 745.
IAEA, *Nuclear Well Logging in Hydrology*, Tech. Report 126, Vienna, 1971.
IAEA, *Commercial Portable Gauges for Radiometric Determination of the Density and Moisture Content of Building Materials*, Tech. Report 130, Vienna, 1971.
G. M. BANCROFT, *Mössbauer Spectroscopy*, J. Wiley, 1973.
J. A. COOPER, Comparison of particle and photon excited X-ray fluorescence applied to trace element measurements on environmental samples, *Nucl. Instr. Methods* **106** (1973) 525.
H. W. THUMMEL, Stand und Entwicklungstendenzen auf dem Gebiet der Isotopen und Strahlenanalytik. Physikalische Analysenverfahren mit Radionukliden, *Isotopenpraxis* **11** (1975)1, 41, 87, 117, 172.
C. H. WANG, D. H. WILLIS, and W. D. LOVELAND, *Radiotracer Methodology in the Biological, Environmental and Physical Sciences*, Prentice Hall, 1975.
W. D. EHMANN, and D. E. VANCE, *Radiochemistry and Nuclear Methods of Analysis*, Wiley Interscience, 1991.
G. FURLAN, P. CASSOLA GUIDA, and C. TUNIZ (Ed.), *New Paths in the Use of Nuclear Techniques for Art and Archeology*, World Scientific Pub., Singapore, 1986.
M. J. RYCROFT (ed.), *The Cambridge Encyclopedia of Space*, Cambridge University Press, 1990